# Limited Scope Report

## Fugitive Dust Emissions: Development of a Real-Time Monitor

SERDP Project RC-1728

OCTOBER 2011

Thomas M. Holsen
Suresh Dhaniyala
Philip K. Hopke
**Clarkson University**

*This document has been cleared for public release*

SERDP
DOD • EPA • DOE

This report was prepared under contract to the Department of Defense Strategic Environmental Research and Development Program (SERDP). The publication of this report does not indicate endorsement by the Department of Defense, nor should the contents be construed as reflecting the official policy or position of the Department of Defense. Reference herein to any specific commercial product, process, or service by trade name, trademark, manufacturer, or otherwise, does not necessarily constitute or imply its endorsement, recommendation, or favoring by the Department of Defense.

# REPORT DOCUMENTATION PAGE

*Form Approved*
*OMB No. 0704-0188*

The public reporting burden for this collection of information is estimated to average 1 hour per response, including the time for reviewing instructions, searching existing data sources, gathering and maintaining the data needed, and completing and reviewing the collection of information. Send comments regarding this burden estimate or any other aspect of this collection of information, including suggestions for reducing the burden, to the Department of Defense, Executive Services and Communications Directorate (0704-0188). Respondents should be aware that notwithstanding any other provision of law, no person shall be subject to any penalty for failing to comply with a collection of information if it does not display a currently valid OMB control number.
**PLEASE DO NOT RETURN YOUR FORM TO THE ABOVE ORGANIZATION.**

| 1. REPORT DATE *(DD-MM-YYYY)* | 2. REPORT TYPE | 3. DATES COVERED *(From - To)* |
|---|---|---|
| 23-05-2011 | Final | Feb 2010 to May 2011 |

**4. TITLE AND SUBTITLE**
Fugitive Dust Emissions: Development of a Real-time Monitor

**5a. CONTRACT NUMBER**
W912HQ-10-C-0025

**5b. GRANT NUMBER**

**5c. PROGRAM ELEMENT NUMBER**

**5d. PROJECT NUMBER**
SERDP RC-1728

**5e. TASK NUMBER**

**5f. WORK UNIT NUMBER**

**6. AUTHOR(S)**
Thomas M. Holsen
Suresh Dhaniyala
Philip K. Hopke

**7. PERFORMING ORGANIZATION NAME(S) AND ADDRESS(ES)**
Clarkson University
Center for Air Resources Engineering and Science
8 Clarkson Ave, Potsdam NY 13699

**8. PERFORMING ORGANIZATION REPORT NUMBER**

**9. SPONSORING/MONITORING AGENCY NAME(S) AND ADDRESS(ES)**
Resource Conservation and Climate Change
SERDP/ESTCP
901 N. Stuart St., Suite 303
Arlington, VA 22203-1853

**10. SPONSOR/MONITOR'S ACRONYM(S)**

**11. SPONSOR/MONITOR'S REPORT NUMBER(S)**

**12. DISTRIBUTION/AVAILABILITY STATEMENT**
Approved for public release; distribution is unlimited

**13. SUPPLEMENTARY NOTES**

**14. ABSTRACT**
The outcome of this project was the development of a real-time instrument (LPI-FM100) that is capable of measuring the particles > 5 micron that make up fugitive dust in real-time. This instrument consists of a commercially available fog monitor (FM-100) (Droplet Measurement Technologies, Boulder CO) connected to an carefully designed and characterized inlet that can sample the large particles typically lost in traditional samplers. The LPI-FM-100 was deployed for a series of intensive field experiments near an unpaved road at a U.S. Army military reservation along-side commercially available samplers. During sampling it was found that there were periods of low particle concentrations interspersed with high concentrations periods that were linked to local traffic. By subtracting the low concentration periods from the high concentration periods a fugitive dust signal was obtained. A significant fraction of the mass was > 10 microns in size. Although these large particles are typically not measured it was found that the LPI-FM100 was able to measure these particles in real-time.

**15. SUBJECT TERMS**
KEYWORDS
Fugitive dust, aerosols, particulate matter, real-time monitors

| 16. SECURITY CLASSIFICATION OF: | | | 17. LIMITATION OF ABSTRACT | 18. NUMBER OF PAGES | 19a. NAME OF RESPONSIBLE PERSON |
|---|---|---|---|---|---|
| a. REPORT | b. ABSTRACT | c. THIS PAGE | | | Thomas M Holsen |
| | | | | | 19b. TELEPHONE NUMBER *(Include area code)* 315-268-3851 |

Reset

**Standard Form 298** (Rev. 8/98)
Prescribed by ANSI Std. Z39.18

# Contents

List of Tables ..... iii
List of Figures ..... iii
List of Acronyms ..... v
Keywords ..... v
Acknowledgements ..... vi
Abstract ..... 1
Objectives ..... 2
Background ..... 3
Materials and Methods ..... 10
Results and Discussion ..... 23
Wind-tunnel LPI characterization. ..... 23
Conclusions and Implications for Future Research ..... 41
References ..... 43
APPENDIX A: Publications ..... 45

## List of Tables

Table 1 Constants used to estimate emissions from unpaved roads (from EPA AP42) .....
Table 2: Field sampling conditions ..... 19
Table 3. Instruments used in the field sampling campaign. The sampling flowrates and size ranges are as provided or recommended by the manufacturer. For the FM-100 the mean bin sizes are 4, 7.5, 10.5, 13.5, 16.5, 19.5, 22.5, 25.5, 28.5, 33, 36, 40, 44, 48, 52, 56, 60, 64, 68, and 73 μm ..... 20

## List of Figures

Figure 1. Size Distribution of particles generated in a laboratory resuspension chamber, TSP stands for total suspended particulate (from Chow et al., 1994) ..... 4
Figure 2. (a) a top view of the LPI without the top lid, (b) side view with 1 cm slit, (c) Clarkson's aerosol wind tunnel,. (d) preliminary results of LPI testing. ..... 6
Figure 3. FM-100 with pump (Droplet Measurements Technology, Boulder, CO.) ..... 8
Figure 4. Schematic diagram of the wind-tunnel experimental setup. ..... 11
Figure 5. APS, LPI-FM-100 and particle injection setup inside the wind tunnel ..... 11
Figure 6: Upstream APS. ..... 12
Figure 7. Characteristics of test particles injected into the wind-tunnel for LPI testing. (a) Data for four specific aerodynamic particle diameters (5.048, 10.37, 14.86, and 19.81μm) binned into 10 seconds time intervals. (b) Particle size distribution measured with the APS during stationary particle injection (10 second average). Error bars represent one standard deviation. ..... 13
Figure 8. (a) The injection heights relative to the inlet locations from where the particles are sampled at a flowrate of 820 LPM. (b) Injection sampling width at a flow rate of 820 LPM relative to the inlet location at a wind speed of 3 m/s. ..... 14
Figure 9. FM-100 and Upstream APS connected by an elbow ..... 15
Figure 10. (a) Schematic diagram of the experimental setup used to disperse glass bead particles into the sample volume of the FM-100 (picture from the FM-100 manual). (b, c) Glass bead size distributions measured by the FM-100 in comparison with off-line measurements made using a Mastersizer instument. ..... 18
Figure 11. A view of the measurement Site 2 and the instruments located at the site. ..... 21
Figure 12. Satellite map of Sites 1 and 2 (From Google maps). ..... 21
Figure 13. The different non-idealities in the sampling systems that must be considered for accurate comparison of experimental results to numerical predictions of LPI sampling efficiency. ..... 23
Figure 14. Enhancement factors for the upstream APS at a wind speed of 1 m/s. ..... 27
Figure 15. Enhancement factors for the upstream APS at a wind speed of 3 m/s. Diffusional and turbulent inertial deposition corrections are not significant for the conditions encountered in these experiments. ..... 27
Figure 16. Enhancement factors for the upstream APS at a wind speed of 4.5 m/s. Diffusional and turbulent inertial deposition corrections are not significant for the conditions encountered in these experiments. ..... 28

Figure 17. Experimental and theoretical elbow factors. Efficiency was calculated by dividing the upstream data by the downstream data (flow rate=820LPM). Error bars indicate one standard deviation. 29
Figure 18. Enhancement factors for the upstream APS at a wind speeds of 1 and 3 m/s. 30
Figure 19. Particle locations in a cross section of tubing downstream of the inlet at 820 LPM showing particles of larger size are not uniform within the sampling tube cross-section. 31
Figure 20. The particle concentration enhancement at central locations downstream of the inlet at 820 LPM. Dp is particle diameter. 32
Figure 21. The particle concentration enhancement at central locations downstream of the inlet at 1750 LPM. 32
Figure 22. A comparion of the numerically predicted inlet enhancements with the experimentally measured values for a sampling flow rate of 820 LPM. The experimental data are corrected for all the measurement non-idealities described above. Error bars indicate one standard deviaiton 33
Figure 23. A comparison of the numerically predicted inlet enhancements with the experimentally measured values for a sampling flow rate of 1750LPM. The experimental data is corrected for all the measurement non-idealities described above. Error bars indicate one standard deviation. 33
Figure 24. Time series of measured size distribution from APS and FM-100. (Aug. 27th). (a) Contour plot of APS data; (b) Contour plot of FM-100 data. Note that the data for both the instruments are plotted in equivalent aerodynamic diameter. A refractive index of 1.51 is used in calculating optical sizes with the FM-100. 35
Figure 25. Particle mass concentration during a day (Aug. 27th). 36
Figure 26. A comparison of $PM_{>10}$ measurements make by the LPI-FM-100 instrument and the filter based technique (TSP-$PM_{10}$). 37
Figure 27. The ratio of PM>10 measurements made by the LPI-FM-100 and the filter-based technique (TSP-PM10) as a function of wind speed. 37
Figure 28. The average total and background particle number size distribution. Particle diameters are aerodynamic diameters for APS and optical diameters for LPI-FM-100. 38
Figure 29. Total and background mass concentration averaged during 10 days. Mass was calculated based on aerodyanmic diameter and unit density for APS, optical diameter and 2 $gm/cm^3$ for LPI-FM-100. 39
Figure 30. The fugitive dust number distribution, averaged for 10 days. 40
Figure 31. The fugitive dust mass distribution, averaged for 10 days. 40

## List of Acronyms

ASME – American Society of Mechanical Engineers
AGU – American Geological Union
APS - Aerodynamic Particle Sizer spectrometer
CFD – computational fluid dynamics
DMT – Droplet Measurement Technology
DoD – Department of Defense
EPA – Environmental Protection Agency
FD – fugitive dust
Hivol – high volume sampler
LPI – large particle inlet
LPI-FM-100 – large particle inlet coupled with a FM-100 instrument
LPM – liters per minute
OAQPS – EPA Office of Air Quality Planning and Standards
PM – particulate matter
TSP – total suspended particulate matter
Stk – Stokes number
VMT - vehicle mile traveled
QA/QC – quality assurance/quality control

## Keywords

Fugitive dust, aerosols, particulate matter, real-time monitors

## Acknowledgements

The authors would like to thank Franklin Page, Environmental Engineer/Air Program Manager at Fort Drum for his invaluable assistance in field sampling, Bruce Gandrud and Droplet Measurement Technologies, Inc for his assistance in operating the FM-100, Dr. Jeffrey Marqusee, SERDP and ESTCP Executive Director, Dr. John A Hall, Program Manager and the HGL staff for their support. Finally we gratefully acknowledge SERDP's financial support.

# Abstract

Objectives. Current efforts to study fugitive dust (FD) are hampered by the lack of an effective, real-time instrument to measure the broad range of particle sizes that make up FD. To meet this need the overall objective of this project was to develop and evaluate a novel instrument capable of measuring, in real-time, ambient concentrations of particles between approximately 2 and 100 μm. This new instrument consisted of a new large particle inlet (LPI) combined with a commercially available particle spectrometer (Droplet Measurement Technology FM-100). The specific objectives of this work were to characterize this new instrument (LPI- FM-100) in a series of laboratory, wind-tunnel and field experiments and compare its performance to traditional, commercially available samplers. The LPI-FM-100 should be able to classify particles into 20 size bins with mean bin sizes between 4 and 73 μm. The instrument should measure a broader range of particle sizes than with those obtained using other techniques to measure large particles.

Technical Approach. This performance of this new instrument (LPI-FM-100) was characterized in the laboratory, in a wind-tunnel and in a series of intensive field experiments at Fort Drum, a U.S. Army military reservation in Jefferson County, New York. Laboratory measurements consisted of aspirating glass beads of known size directly into the FM-100. Wind-tunnel experiments of the new inlet (LPI) mounted on the FM-100 were conducted by measuring upstream and downstream particle concentrations to measure its sampling efficiency. In the field the LPI-FM-100 was deployed alongside traditional filter based particle measurements and other real-time instruments capable of measuring particles up to 20 μm in size. These measurements were compared and the performance of the new sampler evaluated.

Results. Laboratory experiments with glass beads showed that the FM-100 was able to measure particles into 20 size bins and that the measured sizes were consistent with those measured by another light scattering instrument. Wind tunnel measurements found that, as predicted using computational fluid dynamics, the LPI was able to sample large particles at speeds as high as 5 m/s, with sampling efficiency decreasing with particle size and wind speed. During the field measurements it was found that there were periods of low particle concentrations corresponding to traffic-free conditions interspersed with high concentrations periods that were linked to local traffic. After these periods the concentrations quickly returned to background levels after the traffic passed. In the region where size measurements overlap the LPI-FM-100 size distributions were largely consistent with those measured using another real-time instrument. The LPI-FM-100 detected the presence of particles larger than 30 μm during times of traffic movement. A comparison of the filter-based and LPI-FM-100 $PM_{>10}$ values found there is a reasonable match between the measurements made by the two techniques. A first estimation of the fugitive number and mass distribution was obtained from the difference of the background and high concentration periods. This fugitive dust size distribution is mono-modal with a peak at approximatley 8 μm. The fugitive dust size distributions suggest a significant mass concentration of these particles in sizes larger than 10 μm.

Benefits. Overall the findings indicate that military vehicle traffic generates a significant amount of fugitive dust that is highly dynamic and that there are significant peak concentrations near the roadway that quicly returns to background levels. The LPI-FM-100 was able to make fugitive dust concentration measurements in real-time even though much of this dust is larger than can be measured using traditional samplers

## Objectives

Current efforts to study fugitive dust (FD) are hampered by the lack of an effective, real-time instrument to measure the broad range of particle sizes that make up FD. To meet this need the overall objective of this project was to develop and evaluate a novel instrument capable of measuring, in real-time, ambient concentrations of particles approximately 2 to 100 µm. This new instrument consisted of a new large particle inlet (LPI) combined with a commercially available particle spectrometer (Droplet Measurement Technology FM-100). The specific objectives of this work were to characterize this new instrument (LPI- FM-100) in a series of laboratory, wind-tunnel and field experiments and compare its performance to traditional, commercially available samplers. The LPI-FM-100 should be able to classify particles into 20 size bins with mean bin sizes between 4 and 73 µm. The instrument should measure a broader range of particle sizes than with those obtained using other techniques to measure large particles.

## Background

Atmospheric particles originate from a variety of sources and possess a range of morphological, chemical, physical, and thermodynamic properties. Examples include combustion-generated particles, photochemically produced particles, salt particles, and soil-like particles from resuspended dust (EPA, 1996). Airborne particle diameters span more than four orders of magnitude, from a few nanometers to > 100 μm. Combustion-generated particles can be as small as 0.003 μm and wind-blown dust, pollens, plant fragments, and cement dusts are generally above 2 μm in diameter.

Size is one of the most important parameters in determining the properties, effects and fate of atmospheric particles. The atmospheric deposition rates of particles, and therefore their atmospheric residence time, are a strong function of particle size. Light scattering is also strongly dependent on particle size. Particle size distributions, therefore, have a strong influence on atmospheric visibility and through their effect on radiative balance on climate (EPA, 1996).

Windblown dust constitutes a major component of the atmospheric aerosol, especially in arid and semi-arid areas of the world. Windblown dust represents the largest single category in global emissions inventories, constituting about 50% of the total global source of primary and secondary particulate matter (IPCC, 1995).

Fugitive dust (FD) emissions arise from the mechanical disturbance of soils which injects particles into the air. Common sources of FD include vehicles driving on unpaved roads, agricultural tilling, and heavy construction operations. For these sources the dust-generation process is caused by two basic physical phenomena: pulverization and abrasion of surface materials by application of mechanical force through implements (wheels, blades, tracks, etc.) and entrainment of dust particles by the action of turbulent air currents, such as wind erosion of an exposed surface (EPA, 1995).

The impact of a FD source on air pollution depends on the composition and quantity of dust generated and the transport characteristics of the dust particles injected into the atmosphere. Large dust particles often settle out near the source creating a local nuisance problem. Smaller particles are dispersed to much greater distances from the source. The potential transport distance of particles is governed by the initial injection height of the particle, the deposition velocity of the particle, the ambient wind speed and the degree of atmospheric turbulence. Theoretical transport distance, as a function of particle diameter and mean wind speed indicate that, for a typical mean wind speed of 4.4 m/s, particles larger than about 100 μm are likely to deposit within 10 meters from the point of emission. Particles that are 30 to 100 μm in diameter typically deposit within a few hundred meters from the injection point (although under some conditions they can travel significantly farther). Smaller particles can travel long distances because they have much slower deposition velocities and are much more likely to have their settling rate retarded by atmospheric turbulence (EPA, 1995).

Due to the difficulties in estimating windblown dust emissions theoretically, most current estimates rely on the results of empirical studies. These studies typically involve the placement of wind tunnels over natural surfaces and then measuring emission rates and airborne particle size distributions for different wind conditions. The emissions of FD as the result of human activities are also extremely difficult to quantify. Fugitive dust emissions arise from paved and unpaved roads, building construction and demolition, storage piles, and agricultural tilling in addition to wind erosion.

Although the vast majority of recent publications on FD have focused on $PM_{2.5}$ and $PM_{10}$, one recent study investigated the importance of particles > 10 µm in size (Williams et al., 2008). They collected dust on sticky tapes using a rotorod sampler mounted on a tower across an unpaved road. These samples were subsequently analyzed with electron microscopy. These researchers found dust samples from unpaved roads ranged from 0.05 to 159 µm in size and were mostly (70%) silt and clay-sized particles and were collected at all heights. The height and width of the PM plume and the amount of clay-sized particles captured on both sides of the road increased with both vehicle and wind speed.

The complete size distributions of FD from paved and unpaved roads, agricultural soil, sand and gravel, and alkaline lake bed sediments were measured in a laboratory resuspension chamber as part of a study in California (Chow et al., 1994; Figure 1). There is substantial variation in particle size among some of these FD sources although in all cases >40% of the mass was in particles > 10 µm. These particles would not be captured using traditional air samplers.

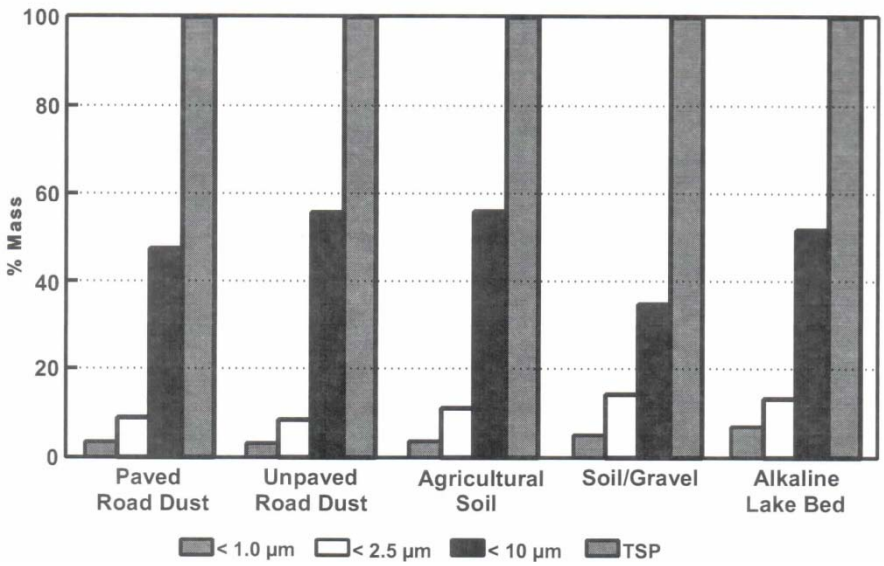


Figure 1. Size Distribution of particles generated in a laboratory resuspension chamber, TSP stands for total suspended particulate (from Chow et al., 1994)

The U.S. EPA AP-42 emission factor (U.S. Environmental Protection Agency, 1995a) for unpaved road dust emissions contains variables which account for silt loading, mean vehicle speed, mean vehicle weight, mean number of wheels, and number of days with detectable precipitation, to determine annual FD emissions for each vehicle-kilometer traveled. The following empirical expression was developed by EPA to estimate the quantity in pounds (lb) of size-specific particulate emissions from an unpaved road, per vehicle mile traveled (VMT): For vehicles traveling on unpaved surfaces at industrial sites, emissions are estimated from Equation 1:

$$E = k\left(\frac{s}{12}\right)^{a}\left(\frac{W}{3}\right)^{b} \qquad \text{Eqn 1}$$

where *k*, *a* and *b* are empirical constants in Table 1 (EPA, AP42) and

$E$ = size-specific emission factor (lb/VMT)

$s$ = surface material silt content (%)

$W$ = mean vehicle weight (tons)

Table 1 Constants used to estimate emissions from unpaved roads (from EPA AP42)

| Constant | Industrial Roads (Equation 1a) | | |
|---|---|---|---|
| | PM-2.5 | PM-10 | PM-30* |
| k (lb/VMT) | 0.15 | 1.5 | 4.9 |
| a | 0.9 | 0.9 | 0.7 |
| b | 0.45 | 0.45 | 0.45 |
| c | - | - | - |
| d | - | - | - |
| Quality Rating | B | B | B |

The source characteristic $s$ is referred to as correction parameter for adjusting the emission estimates to local conditions. The quality rating of B indicates that the tests were judged by EPA to be performed by a generally sound methodology, but lacking enough detail for adequate validation. Using equation 1 and the constants in Table 1 it can be shown that approx. 40% of the mass in fugitive dust is expected to be > 10 µm in size.

**Commercially Available Particle Sampling Instruments.** There are a variety of commercially available particle sampling instruments. Most of them are size-selective which indicates that they collect particles below or within a specified aerodynamic size range, usually defined by the 50% cut point size. These cut-sizes have largely been developed in an effort to measure particle size fractions with some special significance, e.g., health, visibility, source apportionment, etc. The $PM_{10}$ standard set by the U.S. Environmental Protection Agency in 1987 is an example of size-selective sampling (Federal Register, 1987). The $PM_{10}$ size cut was designed to focus regulatory concern on those particles small enough to enter the thoracic region. The upper cut point of $PM_{10}$ samplers, as defined in Appendix J to 40 Code of Federal Regulations (CFR) Part 50 (Federal Register, 1988) have a 50% collection efficiency at 10 ± 0.5 µm diameter. The slope of the collection efficiency curve is defined in amendments to 40 CFR, Part 53.

Prior to the establishment of the $PM_{10}$ standard, the particulate matter standard was based on total suspended particulate matter (TSP). TSP is defined by the design of the High Volume Sampler (hivol). The upper cut off size of the hivol depends on the wind speed and direction but is generally thought to be between 15 and 20 µm. Samplers with upper cut-points of 3.5, 2.5, 2.1 and 1.0 µm are also in use. Dichotomous samplers split the particles into smaller and larger fractions, which may be collected on separate filters.

All of these samplers collect material on filters that must be weighed before and after sampling to obtain the mass of particles collected. In addition to these instruments there are several "real-time" instruments available to measure size-segregated particle concentrations. For example the Model 3321 Aerodynamic Particle Sizer spectrometer (APS) from TSI provides high-resolution,

real-time aerodynamic measurements of particles using light-scattering. The instrument specifications suggest a measurement size range from 0.5 to 20 µm. However, our experience with this instrument suggests that particles greater than approximately 15 µm are removed in the sample tubing and do not enter the instrument for measurement. The TEOM Series 1400ab Ambient Particulate Monitor (Thermo Scientific) makes a direct measurement of particulate mass collected on a filter using a tapered element oscillating microbalance (TEOM) technology. It comes with a choice of sample inlets for PM-10, PM-2.5, PM-1 or TSP monitoring. Mass concentration data is reported in $\mu g/m^3$ at standard averaging times of 10 min, 30 min, 1, 8, and 24 hours.

**PM Regulations.** At Department of Defense (DoD) sites FD is created by vehicle and aircraft maneuvers, artillery/missile backblast, range maintenance and construction activities, and wind erosion on disturbed surfaces. The amount of FD generated depends on the properties of the soil, the method and intensity of suspension, and prevailing meteorological conditions. The air *quality impacts of these emissions may impair the full use of military installations, particularly*

(a)

(c)

(b)

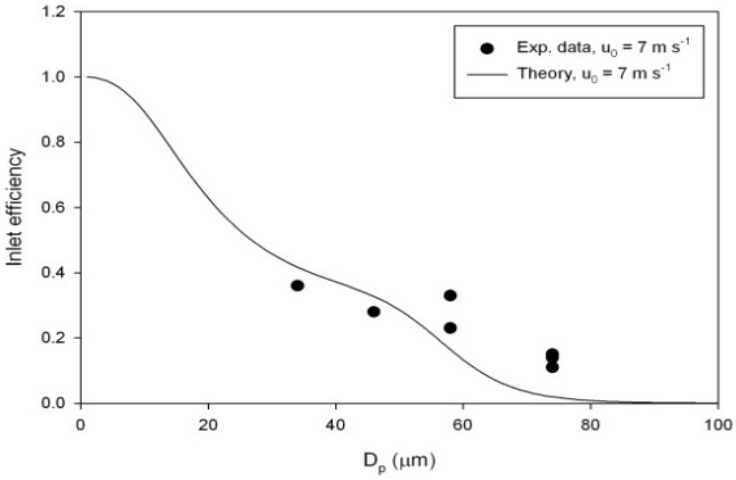


(d)

Figure 2. (a) a top view of the LPI without the top lid, (b) side view with 1 cm slit, (c) Clarkson's aerosol wind tunnel,. (d) preliminary results of LPI testing.

*in* areas that are in nonattainment with the National Ambient Air Quality Standards (NAAQS) for $PM_{10}$ and $PM_{2.5}$.

Although currently only particles <10 µm in size are regulated as ambient particulate matter (PM), there are secondary standards for total suspended particulates (TSP) with includes both $PM_{10}$ and $PM_{>10}$. There is also a standard for lead in TSP. For other toxic metals such as Cr(VI), the National Air Toxics Trends Network also collects TSP samples since nasal deposition and uptake through the gastrointestinal tract represents an important exposure/dose pathway. Since all particle sizes impact visibility, have negative health effects, and can cause negative aesthetic impacts, the complete range of FD particle sizes generated by DoD activities needs to be understood.

Resuspension of FD from contaminated surfaces may also contribute to an increase in the toxic trace elements in airborne particles (Kitsa et al., 1992; Kitsa and Lioy, 1992; Pastuszka and Kwapulinski, 1988; Falerios et al., 1992). Kitsa et al. (1992) measured elemental concentrations in particles resuspended from a waste site in New Jersey. Close to the resuspension source, coarse particles ($PM_{2.5\text{-}10}$) were dominant, but farther downwind from the site, fine particle ($PM_{2.5}$) concentrations were greater than coarse particle concentrations. Particles were enriched in chromium and lead, indicating the potential for elevated human exposure through inhalation. Chromium may exist in different valence states, but the most stable and abundant are the trivalent and hexavalent states. Hexavalent chromium is classified as a known respiratory carcinogen in humans.

**Large Particle Sampling.** There are several established criteria for representative sampling of ambient aerosol (Belyaev and Levin, 1974; Vincent, 1989; Hangal and Willeke, 1990). In general, it is accepted that isoaxial and isokinetic conditions result in representative sampling of aerosol particles from most environments (Gysels and Grieken, 1999). It is, however, usually very difficult to satisfy these conditions because of constantly changing wind speeds and wind directions. This difficulty is compounded for large particles because of their significant inertia and gravitational velocity.

Typically inlets sample anisokinetically, which requires that the relationship between inlet efficiency, geometry, and flow parameters be established prior to its deployment. Inlet efficiency is defined as the ratio of the particle concentration delivered to the aerosol measurement section of the sampler to that in the ambient. The net inlet efficiency is dependent on both the aspiration and transmission efficiency. Aspiration efficiency is the ratio of the aspired particle concentration to that present in ambient air. Transmission efficiency is the ratio of the particle concentration transmitted to the sampling section to that aspired into the inlet.

Aspiration efficiency depends strongly on particle inertia which can be characterized by their Stokes number (Stk) given by:

$$Stk = \frac{\rho_p C_c D_p^2 U_o}{18 \mu W_i} \qquad \text{Eqn 2}$$

where $\rho_p$ is the particle density, $C_c$ is slip correction, $D_p$ is the particle diameter, $U_o$ is the wind velocity, $\mu$ is the gas viscosity, and $W_i$ is a characteristic diameter (slit width in this study). Particles with Stokes numbers larger than ~ 0.3 will not exactly follow turning streamlines causing differences between the sampled and ambient particle concentrations (Dhaniyala et al, 2003).

The criteria for representative aerosol sampling have been established using aspiration and transmission efficiencies as a function of Stk, iso/aniso axial, and iso/anisokinetic conditions (Belyaev and Levin, 1974; Vincent, 1989; Hangal and Willeke, 1990). In this study, the combination of aspiration and transmission efficiencies, referred to as inlet efficiency, of the LPI-FM-100 will be established experimentally as a function of particle size and free stream wind speed ($U_o$).

**Large particle inlet (previously designed and tested).** To accurately sample $PM_{>10}$, a new inlet was recently designed in our group (Lee et al., 2008). This inlet, called the Large Particle Inlet (LPI), is designed for sampling large particles over a wide range of wind velocities, independent of wind direction (Figure 2). In the LPI, air is sampled via a narrow circular slit into a funnel-shaped section that turns the sampled flow to a vertical direction, facilitating effective post-sampling analysis. The optimal inlet design was arrived at using computational fluid dynamics (CFD) modeling.

The inlet performance as a function of its funnel geometry, operating parameters, and the ambient wind conditions was numerically determined. The size of the sampling circumferential slit and the shape of the funnel were observed to critically determine the inlet performance. A narrow slit width is used at the entrance of the LPI to ensure omnidirectional sampling, while an elliptical funnel section shape is used to ensure that the sampled air is transported with minimal recirculation through the inlet. The omni-directional entrance provides a counter-flow effect that aids turning of large particles from the horizontal sample plane to the vertical exit port. Effective operation of the LPI requires a sampling flowrate greater than 1000 LPM. The LPI efficiencies are dependent on inlet geometry, particle sizes, sample flowrate, and ambient wind speeds. At an ambient wind speed of 7 m/s, the LPI design with a 1cm slit width entrance is predicted to have a sampling efficiency greater than 40% for particles as large as 50µm. The upper cut-size and inlet efficiencies are dependent on the ratio of ambient wind speed and the sample flow velocity at the entrance slit.

Figure 3. FM-100 with pump (Droplet Measurements Technology, Boulder, CO.)

The final fabricated inlet is shown in Figures 2a and b. Initial testing of the inlet was conducted in Clarkson University's aerosol wind-tunnel (Figure 2c) using polydispersed Arizona road dust particles (Powder Technology Inc (PTI), MN) as test aerosol. The initial results provide reasonable validation of the inlet performance.

As a part of this project, we conducted extensive wind-tunnel based experimental analysis of the LPI performance as a function of wind-speed and particle diameter. For real-time measurement of large particles (particularly particle diameters larger than 10 μm), the LPI was integrated with a FM-100 instrument (Figure 3). The integrated LPI-FM-100 instrument was evaluated with field experiments and particle size distribution measurements of fugitive dust made with this integrated instrument suggest that particles as large as 30 μm are common near unpaved roads.

## Materials and Methods

The deployment of the LPI-FM-100 system for measurement of large particle size distributions and concentrations requires its prior validation with appropriate laboratory and field experiments. The different components of the experimental validation effort included:

1) Wind-tunnel based testing and validation of the performance of the LPI sampling efficiency,
2) Lab-based testing of FM-100 sizing performance, and
3) Field based validation of size distribution measurements by the integrated LPI-FM-100.

The details of above experimental components are provided below.

**Wind Tunnel Testing.** Wind tunnel tests were performed to establish the sampling characteristics of the large particle inlet (LPI). The experiments were conducted in Clarkson's Aerosol Wind-tunnel which has a test section with cross-sectional dimensions of 122 cm x 91cm. The experimental procedure for wind-tunnel testing included:

1) Ensuring uniform particle seeding in the wind-tunnel, and
2) Characterizing the performance of the LPI using identical real-time particle sensors for upstream and downstream measurements.

The following instruments were used in the wind-tunnel experiments

**Dust Feeder (Particle injection).** The wind-tunnel was seeded with Arizona Road Dust (ARD; Powder Technology Inc.) dispersed using a Topas Solid Aerosol Generator 410 (Topas Gmbh, Dresden, Germany). The Topas dust generator ejects solid particles as large as 100 µm continuously, consistently, and reproducibly.

**Aerodynamic Particle Sizer (APS) (flow rate 5LPM)**. Two APS (Model 3321; TSI Inc.) units were used to determine the real-time particle concentrations upstream and downstream of the LPI. The APS instrument uses a double-crest optical system to detect the time-of-flight of particles exiting a nozzle and analyzes the signal to determine particle aerodynamic diameter over a size range of 0.5 to 20 µm. The use of two identical real-time units for upstream and downstream measurements enables easy characterization of LPI performance while using a time-varying injection system described below.

**Wind Tunnel Testing Procedures.** Time-averaged uniform seeding of the aerosol wind tunnel was obtained by injecting particles through a downward-facing vertical copper tube mounted downstream of a small turbulent grid connected to the dust feeder (Figure 4 and Figure 5). This tube and grid were mounted on a two-dimensional traverse system, enabling the precise movement of the injection location about the tunnel. The injection point was generally moved on a serpentine path 63.5 cm horizontally and 25.4 cm vertically in vertical steps of 0.64 cm. The entire motion takes approximately 30 minutes to complete.

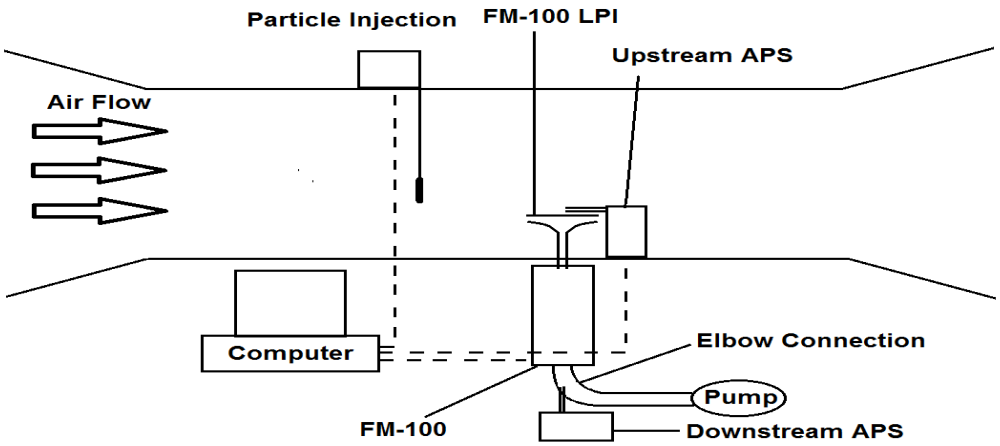


Figure 4. Schematic diagram of the wind-tunnel experimental setup.

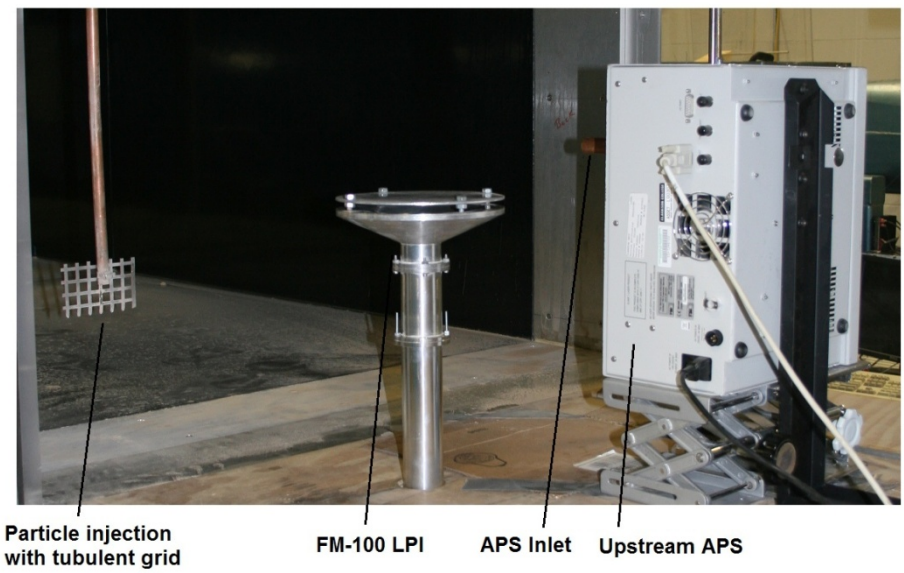


Figure 5. APS, LPI-FM-100 and particle injection setup inside the wind tunnel.

To determine that the dust feeder was delivering a constant particle supply, real-time particle size distributions were measured using the APS instrument placed in the wind tunnel with the sampling tube facing upstream into the flow seeded by the dust feeder without movement of the injection system (Figure 6). Coarse Arizona Road Dust (ISO 12103-1, A4 Coarse Test Dust, Powder Technology Inc.) was used as the test aerosol. Analysis of APS particle concentrations binned into 10 second intervals suggest that, in approximately thirty minutes of testing, the APS concentrations were fairly constant (Figure 7). The size distributions of the generated particles were such that approximately 80 particles $cm^{-3}$ were generated at the smallest particle sizes of interest (2μm) and concentrations monotonically decreased to ~ 0.5 particles $cm^{-3}$ for the largest particles measured by the APS (20 μm). Over the sampling period the standard deviation of particle number concentrations ranged from 17.6 (2.2 μm) to 0.107 (19.8 μm) (Figure 7).

Figure 6: Upstream APS.

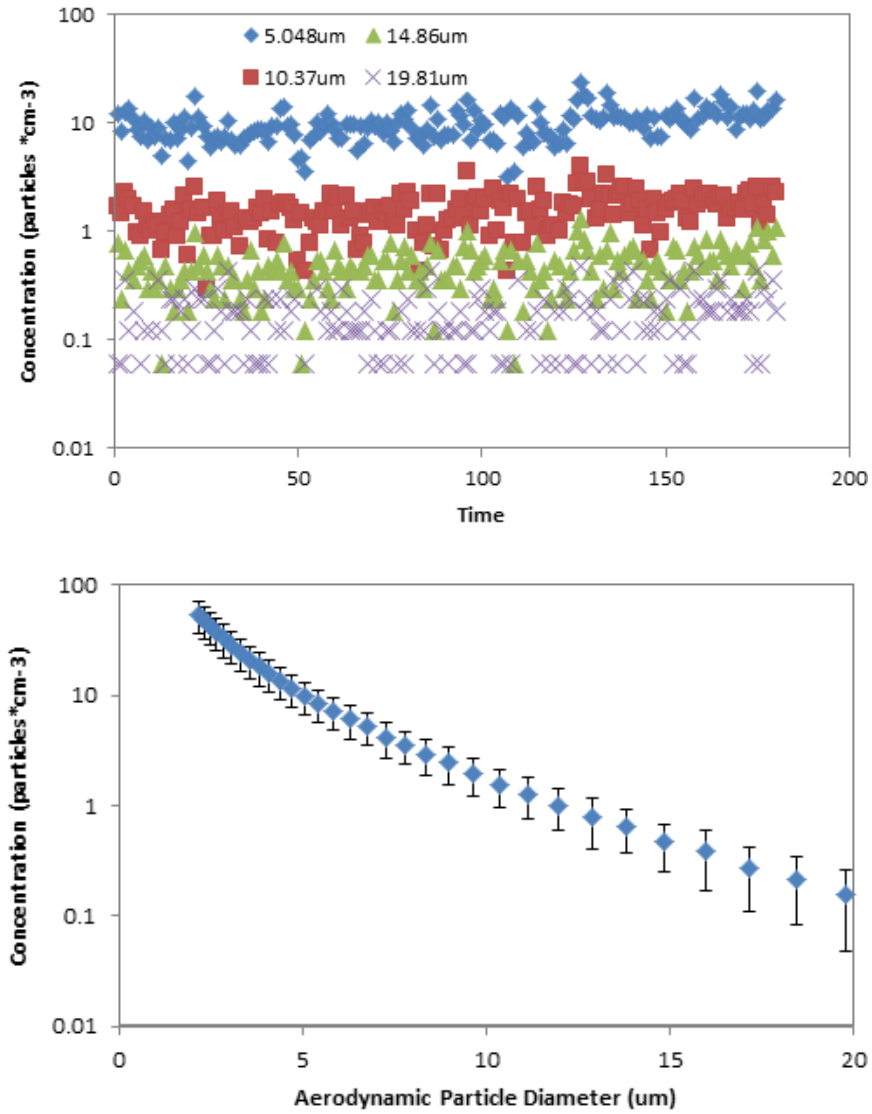


Figure 7. Characteristics of test particles injected into the wind-tunnel for LPI testing. (a) Data for four specific aerodynamic particle diameters (5.048, 10.37, 14.86, and 19.81µm) binned into 10 seconds time intervals. (b) Particle size distribution measured with the APS during stationary particle injection (10 second average). Error bars represent one standard deviation.

To ensure that the particle seeding in the tunnel spanned the entire sampling volume of the LPI, the dust feeder outlet was moved vertically and horizontally about the centerline of the inlet until the injected particles were outside the sample flow region of the LPI. This experiment was repeated for winds speeds of 1, 3, and 5 m/s. As expected the sampling volume height decreased with increasing wind speed from approximately 80 cm at 1 m/s to 40 cm at 5 m/s (Figure 8). The width of the sampling volume was ~ 16 cm at a wind speed of 3 m/s. The sampling region width was considerably smaller and less dependent on wind speed than the range of sampling heights (Figure 8). In all subsequent inlet tests at least this area upstream on the inlet was seeded.

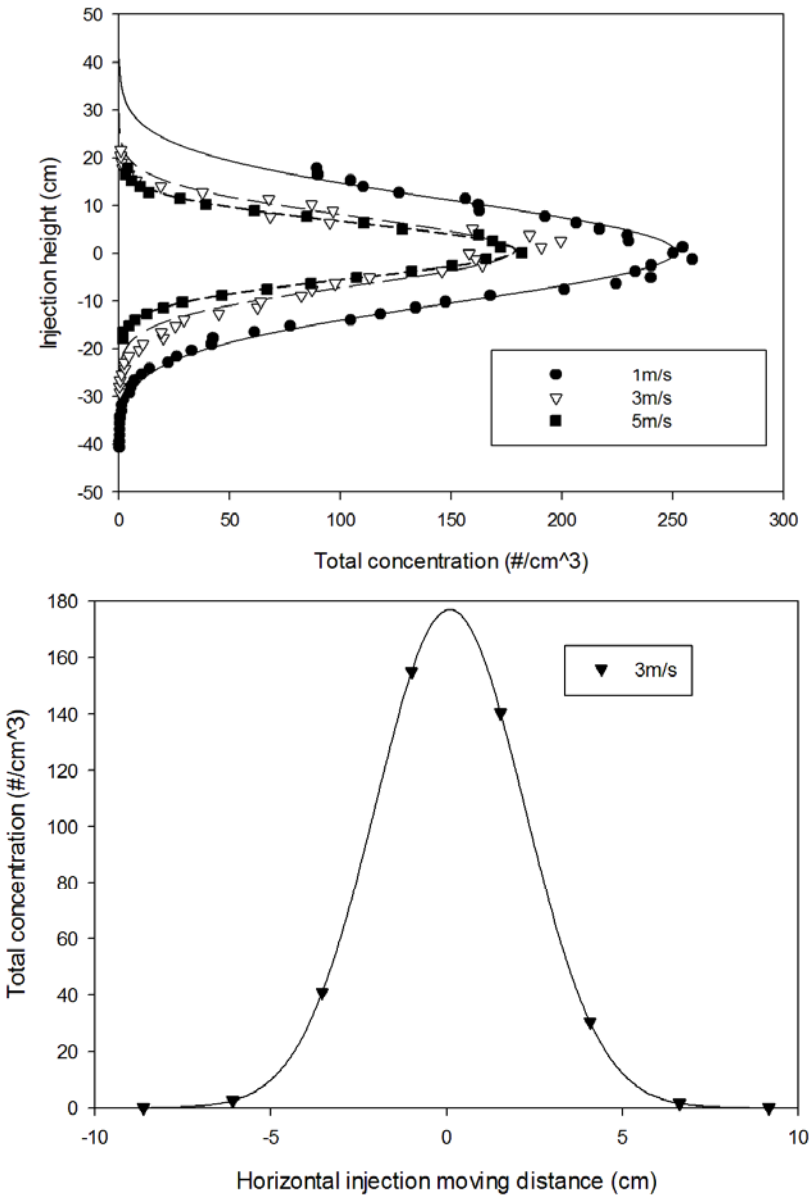


Figure 8. (a) The injection heights relative to the inlet locations from where the particles are sampled at a flowrate of 820 LPM. (b) Injection sampling width at a flow rate of 820 LPM relative to the inlet location at a wind speed of 3 m/s.

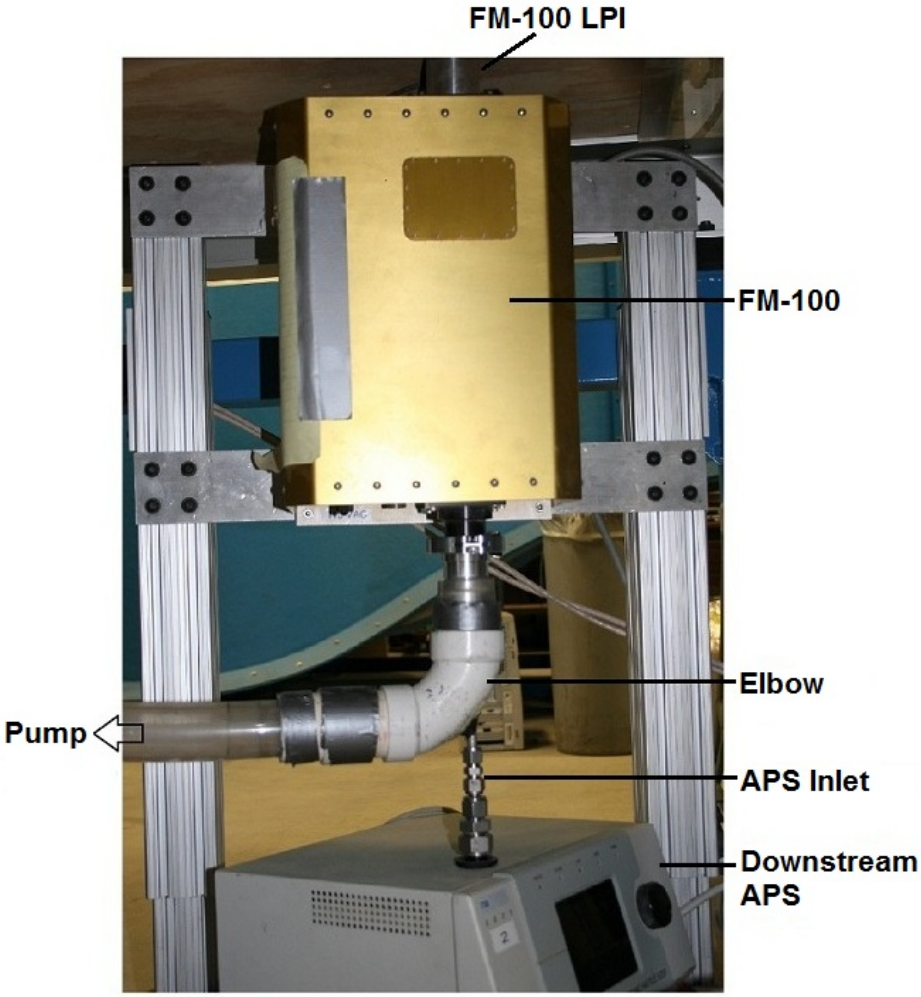


Figure 9. FM-100 and Upstream APS connected by an elbow.

**LPI Testing:**

To determine the LPI sampling efficiency, an APS was placed inside the wind tunnel (upstream APS) to measure the upstream particle concentration, and another APS (downstream APS) was placed downstream of the LPI. The downstream APS sub-sampled from the flow exiting the LPI through an elbow as shown in Figure 9. Measurement of particle concentrations downstream of the LPI were made with a second APS rather than directly by the FM100, because a direct comparison of two APS measurements provides a direct measurement of LPI sampling efficiency without the need to convert optical particle sizes to aerodynamic sizes. For these experiments, the particle injection system traveled from left to right 63.5 cm, and was stepped 0.64 cm in height after each pass for 45 passes (total height 28 cm) for a wind speed setting of 1m/s. For wind speeds of 3 and 4.5 m/s, a total 41 passes were used (total height 25.4cm). Two flow rates were used in these tests (820 and 1750 LPM) since previous experiments have shown that the inlet efficiency is flow rate dependent.

**FM-100 testing.**

**Fog Monitor** (FM-100; flow rate: 820 Liters per minute (LPM)). The sizing performance of the FM-100 was tested with glass bead particles in a bench-top laboratory experimental setup. The FM-100 uses a light scattering technique to determine the size and number of particles passing through a sample volume (Figure 3). In the FM-100, as particles pass through a laser beam, photons are scattered in all directions and the cone of photons that are forward scattered in the 4° to 12° range are collected and directed onto a 1:2 optical beam splitter, and then to a pair of photodetectors. The photodetectors convert the photon pulses into electrical pulses. One photodetector sees 33% of the collected light and one photodetector sees the 67% of the light collected from the particles that pass through the laser beam if and only if, the scattered light is collected and focused through the optical mask. The instrument has an upper-cut size in the range of 70 μm after which size the instrument begins to lose resolution. The smallest particle detection by the FM-100 is 2 μm and the mean bin sizes are 4, 7.5, 10.5, 13.5, 16.5, 19.5, 22.5, 25.5, 28.5, 33, 36, 40, 44, 48, 52, 56, 60, 64, 68, and 73 μm.

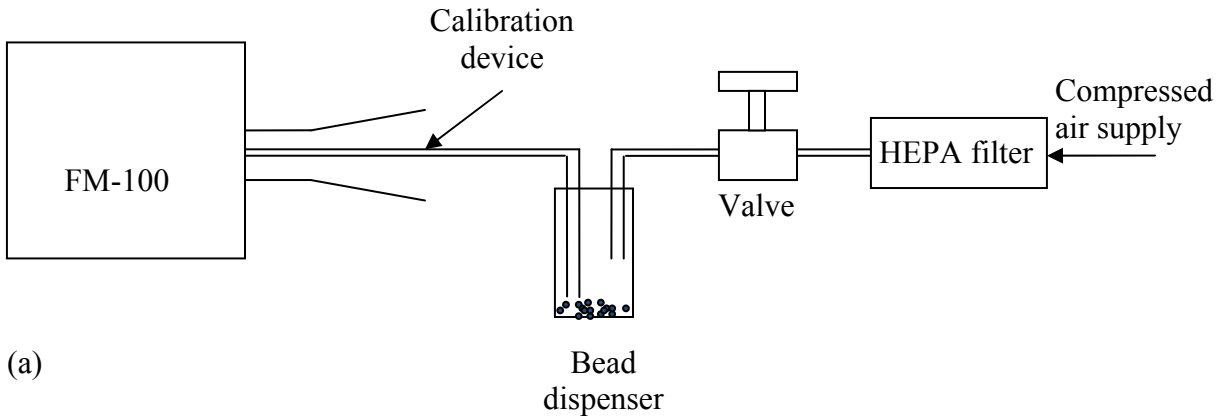
Calibration device
FM-100
Compressed air supply
HEPA filter
Valve
Bead dispenser

(a)

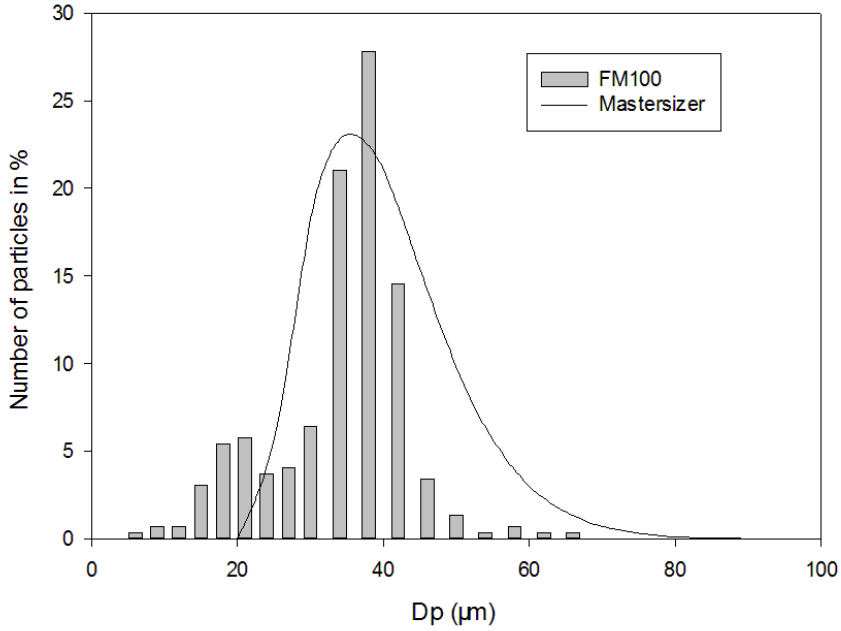
FM100
Mastersizer
Number of particles in %
Dp (µm)
0
5
10
15
20
25
30
0
20
40
60
80
100

(b)

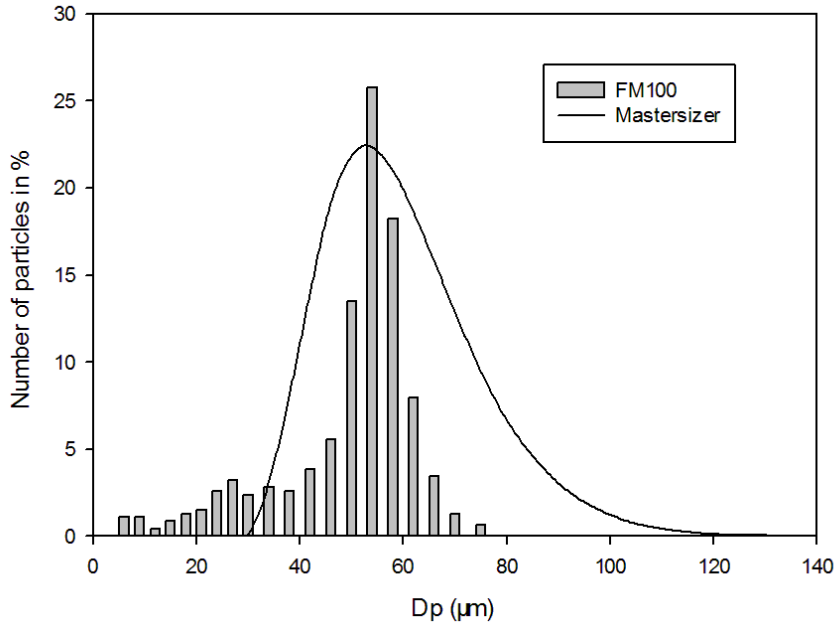


(c)

Figure 10. (a) Schematic diagram of the experimental setup used to disperse glass bead particles into the sample volume of the FM-100 (picture from the FM-100 manual). (b, c) Glass bead size distributions measured by the FM-100 in comparison with off-line measurements made using a Mastersizer instument.

To test the performance of the FM-100, several lab-based tests were conducted by aspirating glass bead particles of different sizes directly into the FM-100 using the experimental setup shown in Figure 10a. The test particles were placed in a bead dispenser glass bottle and a "puff" of air was introduced into the bottle using a compressed air source and an on/off valve. Repeated measurements were made to ensure accurate determination of size distribution of the dispersed particles and the average values obtained from these measurements is shown in Figures 10b and 10c. To confirm the size of the glass bead particles, offline size distributions of the test particles were made by dispersing a small sample of these particles in a 5 mL water container and measuring their size distributions using a light scattering instrument (Mastersizer 2000, Malvern, Inc). These tests indicated that the average sizes measured by FM-100 were consistent with those obtained from the Mastersizer measurements. The size distributions obtained from the two instruments, however, differed in the lower and higher limits of the distribution. Relative to the Mastersizer measurements, the FM-100 size distributions show an increased presence of particles smaller than the mean size and decreased presence of particles larger than the mean size. This discrepancy is likely because of the different dispersion mechanisms used for the two samples. For the off-line measurements, particles were dropped into water and dispersed using a ultrasonic bath, while the particles were dispersed into the FM-100 using a compressed air source, which is likely to result in a higher dispersion efficiency of smaller particles than larger particles.

**Field tests for LPI-FM-100:**

The laboratory experiments described above validate the sampling characteristics of the LPI and the sizing capability of the FM100. Wind-tunnel testing of the integrated LPI-FM-100 was not

directly possible because only one FM-100 instrument was available, complicating comparison of upstream and downstream measurements. The use of non-identical instruments such as the APS and the FM-100 for upstream/downstream measurements were complicated by the very different sizing and concentration detection limits of these instruments. Thus, the integrated LPI-FM-100 instrument was calibrated with a field measurements in conjunction with traditional sampling devices as described below.

**Field Sampling Methods.** Field experiments were conducted at two sites in Fort Drum, NY (Figures 11 and 12). One site (Site 1) was located inside the military base at the edge of a parking lot adjacent to an unpaved road. A variety of vehicles utilized the road including motorcycles, sedan cars and 18-wheel trucks. The other site (Site 2) was also adjacent to an unpaved road that was used as a convoy route near a water treament plant and water. Most of the vehicles that passed this site (Site 2) were military trucks; no tracked vehicles passed during the sampling period. There are no industrial or residental air pollution sources near the sampling area. The test dates were: Aug. 17$^{th}$ to 19$^{th}$ at site 1; Aug. 24$^{th}$ to 27$^{th}$ and Aug. 30$^{th}$ to Sept.1 at site 2. All in 2011. The measurements at these sites were typically made from 8:30 AM to 4:00 PM during the test dates.

Table 2. Field sampling conditions

| Date | Day | Location | Instrument Used | Sampling Time |
|---|---|---|---|---|
| Aug. 17$^{th}$ | 1 | Site 1 | All except Dichot, Dusttrak and MOUDI | 5 hours 30 minutes |
| Aug. 18$^{th}$ | 2 | Site 1 | All except Dusttrak and MOUDI | 6 hours 30 minutes |
| Aug. 19$^{th}$ | 3 | Site 1 | All except Dichot, Dusttrak and MOUDI | 4 hours 15 minutes |
| Aug. 24$^{th}$ | 4 | Site 2 | All except Dichot, Dusttrak and MOUDI | 5 hours 30 minutes |
| Aug. 25$^{th}$ | 5 | Site 2 | All | 6 hours 15 minutes |
| Aug. 26$^{th}$ | 6 | Site 2 | All | 5 hours 30 minutes |
| Aug. 27$^{th}$ | 7 | Site 2 | All | 5 hours 50 minutes |
| Aug. 30$^{th}$ | 8 | Site 2 | All | 6 hours 20 minutes |
| Aug. 31$^{st}$ | 9 | Site 2 | All | 6 hours 10 minutes |
| Sept. 1$^{st}$ | 10 | Site 2 | All | 5 hours 50 minutes |

**Instrumentation.** The instruments used to take samples are listed below in Table 3. The Federal Reference Method (FRM) and Dichot samplers collect particles on Teflon filters. The Micro-Orifice Uniform Deposition Impactors (MOUDI) collects particles on a metal substrate. The sampled particle mass was evaluated by determining the weight difference between the tare and sample weight. For the real-time samplers the APS (Aerodynamic Particle Sizer, TSI 3321) uses time-of flight techniques to measure the particle aerodynamic diameter; the.Fog Monitor (FM-100) with large particle inlet (LPI) (LPI-FM-100) uses light scattering techniques to detect and size the sampled particles and the Dusttrak with 2.5µm inlet (TSI 8520) uses light scattering techniques to measure the particle mass concentration

Table 3. Instruments used in the field sampling campaign. The sampling flowrates and size ranges are as provided or recommended by the manufacturer. For the FM-100 the mean bin sizes are 4, 7.5, 10.5, 13.5, 16.5, 19.5, 22.5, 25.5, 28.5, 33, 36, 40, 44, 48, 52, 56, 60, 64, 68, and 73. μm

| **Instrument** | **Measurement** | **Time resolution** | **Size range (μm)** | **Sample flowrate (LPM)** |
|---|---|---|---|---|
| APS TSI 3321 | Aerodynamic size distributions | 1 sec | 0.5-20 | 5 |
| FRM TSP | Mass | N/A | < 100 | 16.67 |
| FRM $PM_{2.5}$ | Mass | N/A | < 2.5 | 16.67 |
| FRM $PM_{10}$ | Mass | N/A | <10 | 16.67 |
| Dichot | Mass | N/A | <2.5, 2.5-10 | 16.67 |
| MOUDI | Mass Distribution | N/A | < 30 | 30 |
| LPI-FM-100 | Optical size distribution | 1 sec | 2-75 | 1000 |
| Dusttrak TSI 8520 | Real-time photometric based total mass concentration | 5 sec | 0.3-2.5 | 3 |

The instruments were placed on individual platforms that ensured that the sampling heights of all the instrument inlets were at the same height (approximately 2 m off the ground). Some notes about the measurements:

1) The Dusttrak was placed with its sampling tube pointing upright.
2) The LPI-FM-100 and APS were operated at a sampling rate of 1 second as recommend by the manufacturers.. The LPI-FM-100 reports the particle counts for each size bin from an optical size of 6 to 75μm.
3) Aerosol instrument management software from TSI was used to capture the APS data.
4) The Dusttrak sampling interval was set to 5 seconds as is recommended for the concentrations encountered.
5) The Teflon filters used in the FRM and Dichot were pre-weighted in a cleanroom with a microgram scale. On each sampling day, one filter travel blank for each instrument was used. At the end of each day, all the filters were removed from the instruments with the holders, individually packed into petri dishes and sent back to the cleanroom.

The traffic patterns at the sampling sites were not controlled and were generally random; however, in general there were more vehicles observed to pass the sites around noon each day.

Figure 11. A view of the measurement Site 2 and the instruments located at the site.

Figure 12. Satellite map of Sites 1 and 2 (From Google maps).

A comparison of the mass measured by the LPI-FM-100 for particles larger than 10 μm with that obtained from filter based measurements (difference of TSP and PM10 measurements) provide

an initial validation of the ability of the LPI-FM-100 instrument to detect and characterize the particle fraction larger than 10 μm.

## Results and Discussion

**Wind-tunnel LPI characterization.** Validation of the LPI sampling efficiency performance requires the comparison of experimental efficiency results (obtained as a ratio of APS concentrations downstream and upstream of the inlet) with the numerically obtained values of Lee et al., (2008). For comparison of the LPI-FM-100 experimental results to numerical predictions, the obtained data must first be corrected for the experimental non-idealities, such as anisokinetic sampling, and particle sedimentation losses. A schematic diagram illustrating the primary locations of sampling non-idealities is shown in Figure 13 and the approach to address the different non-idealities is discussed below.

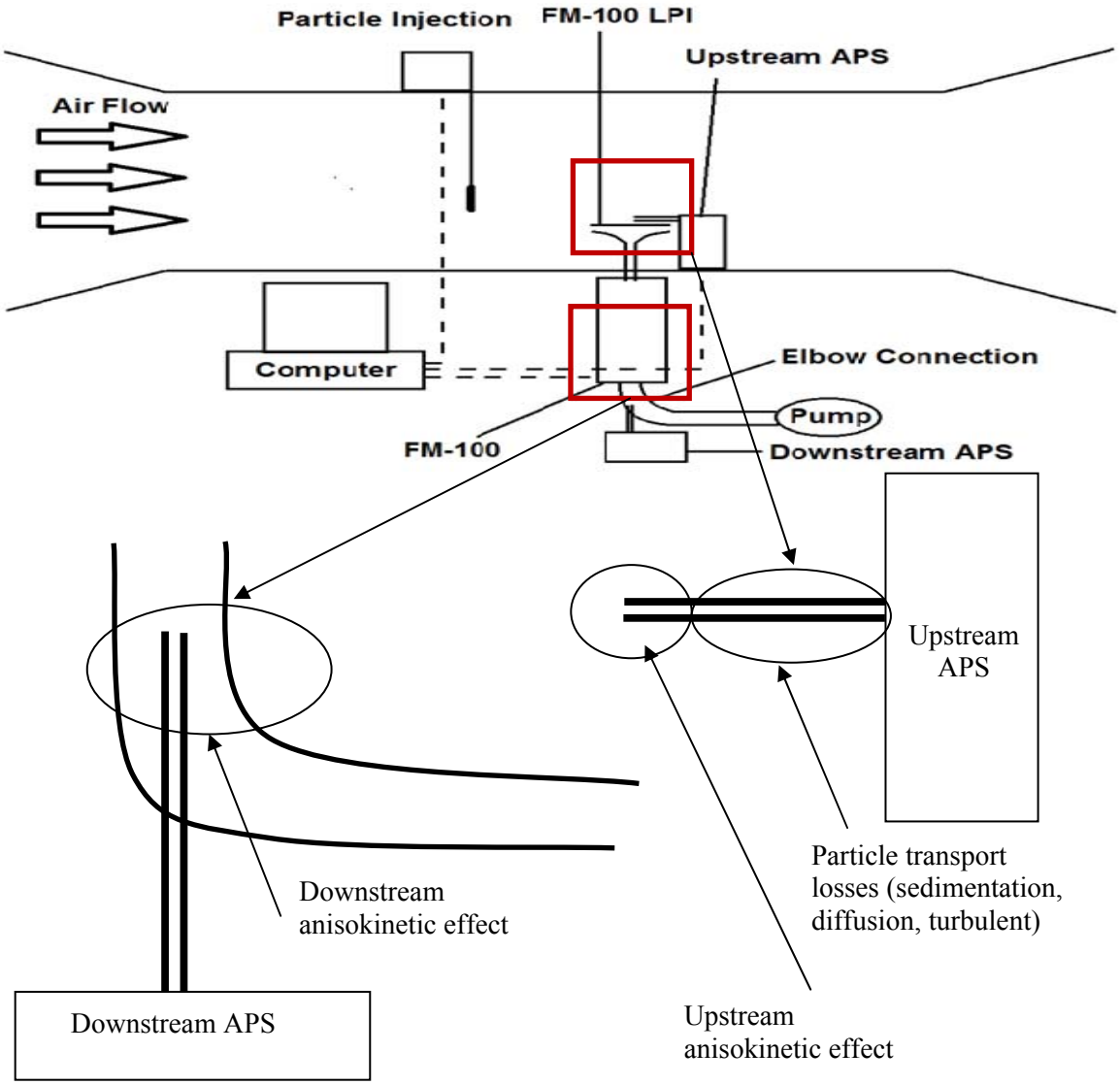


Figure 13. The different non-idealities in the sampling systems that must be considered for accurate comparison of experimental results to numerical predictions of LPI sampling efficiency.

**Downstream APS: Anisokinetic sampling effect.** The APS has a small sample flowrate of 5 LPM relative to the LPI sampling flowrate of ~ 1000 LPM. A small amount of flow must, thus, be sub-sampled to the APS and this flow must be transported vertically to the APS to minimize losses of large particles during transport. Vertical sub-sampling from the bulk-flow is achieved using an elbow assembly shown in Figure 13. Ideally, the APS sub-sample flow can be extracted isokinetically (i.e., identical sampling and free-stream velocities) from the LPI flow, but the large difference in the flowrates of the APS and the LPI, makes this difficult to achieve. Non-isokinetic (anisokinetic) sampling results in particle concentration enhancements where the concentration in the sampled air is greater than the average concentration in the sample tube. In this situation concentrations of particles of different sizes are enhanced differently. The extent of enhancements can be calculated from the semi-empirical expression of Belyaev and Levin (1975).

**<u>Anisokinetic enhancement</u>**

The theoretical anisokinetic enhancement factor can be determine using the relationship (Belyaev and Levin, 1975)

$$E_{aniso} = 1 + \left(\frac{U_0}{U} - 1\right) * \left(1 - \frac{1}{1+B*Stk}\right) \qquad \text{Eqn 3}$$

where, $U_0$ is the free stream velocity, U is the sample velocity, the constant, B is given as:

$$B = 2 + \frac{0.617}{(U_0/U)} \qquad \text{Eqn 4}$$

and Stk is the particle Stokes number, defined as:

$$Stk = \tau * U_0/D_{tube} \qquad \text{Eqn 5}$$

Where the particle relaxation time, τ, can be calculated as (Hinds, 1999)

$$\tau = \frac{\rho_p D_p^2 C_C}{18\mu} \qquad \text{Eqn 6}$$

where $\rho_p$ is the particle density, $D_p$ is the particle diameter (um), μ is flow viscosity,, and $C_c$ is Cunningham correction factor.

$$Cc = 1 + \left(\frac{2}{(P*Dp*0.7502)}\right) * (6.32 + 2.01 * exp(-0.1095 * P * 0.7502 * Dp)) \qquad \text{Eqn 7}$$

where P is the pressure (=101.325kPa).

A comparison of the experimental and theoretical elbow factor shows that for a sample flow rate of 1750LPM, the experimentally obtained enhancements in the downstream APS data are somewhat higher than the theoretically calculated values for particle diameters between 2μm and

20 μm. The theoretical efficiency is somewhat lower than measured values, particularly at the smaller particle sizes. For a LPI sample flowrate of 820LPM, the measured elbow factors are somewhat higher than the theoretical value for diameter smaller than 12 μm and slightly lower at higher diameters.

**Transport losses for the upstream APS.**

**Sedimentation:** The upstream APS (Figure 6) samples through a 20.32cm horizontal tube facing the flow. During transport in this tube, prior to entering the APS detector, some particles may be lost to the wall of the tube due to gravitational sedimentation. This possibility was considered by the threotical expression for sedimention penetration efficiency, $P_{sed}$ (Pich, 1972):

$$P_{sed} = 1 - \frac{2}{\pi}[2\varepsilon\sqrt{1-\varepsilon^{2/3}} - \varepsilon^{1/3}\sqrt{1-\varepsilon^{2/3}} + sin^{-1}\varepsilon^{1/3} \qquad \text{Eqn 8}$$

Where

$$\varepsilon = 0.75 * Vs/(2 * R) * (L_{\ hori-tube}/U_0) \qquad \text{Eqn 9}$$

where $V_s$ is the settling velocity determined as:

$$Vs = \tau * g \qquad \text{Eqn 10}$$

and $L_{hori\text{-}tube}$ = 20.32cm, and $U_0$ is the free stream velocity (wind speed).

The sedimentation losses in the tube result in an enhancement value of < 1 for all size particles and the importance of this factor increases with particle size to an enhancement value of approximately 0.52 for 20 μm particles. This value depends only on the residence time in the inlet tube so it is independent of wind speed.

**Diffusional deposition.** During transport of particles in the horizontal sampling tube upstream of the APS, some particles may be lost to the wall of the tube due to diffusion. The efficiency of particle transport under diffusion can be calculated as (Gormley and Kennedy, 1949):

$$E_{diff} = 1 - 2.56 * \delta^{2/3} + 1.2 * \delta + 0.177 * \delta^{4/3} \qquad \text{When } \delta < 0.02 \qquad \text{Eqn 11}$$

$$\text{Or } E_{diff} = 0.819\exp(-3.657\delta) + 0.097\exp(-22.3\delta) + 0.032\exp(-57\delta) \qquad \text{Eqn 12}$$
$$\text{When } \delta > 0.02$$

where

$$\delta = \frac{DL}{U_s R^2} \qquad \text{Eqn 13}$$

where D is particle diffusion coefficient ($cm^2/s$), L is the tube length (20.32cm), $U_s$ is sampler velocity, R is radius of tube, K is Boltzman constant (=1.38E-16 erg/K). This correction is not significant for the conditions encountered in these experiments (Figures 16-18).

**Turbulent inertial deposition.** During transport through the inlet tube of the APS to the detector particles may impact on the walls due to the turbulence. This possibility was evaluated using the following approach (Liu and Agarwal, 1974).

$$Re = \frac{\rho_a U_s D_{tube}}{\mu} \qquad \text{Eqn 14}$$

$$T=0.0395*Stk*Re^{0.75} \qquad \text{Eqn 15}$$

$$V_t = 6E\text{-}4*T^2 \quad \text{when } T<12.9 \qquad \text{Eqn 16}$$

$$\text{Or } V_t=0.1 \qquad \text{Eqn 17}$$

Where $\rho_a$ equals air density ($=1.2*10^{-3}$ $g/cm^3$). This correction is not significant for the conditions encountered in these experiments.

**Anisokinetic sampling.** Similar to the downstream APS anisokinetic enhancement factor discussed above the velocity difference between the inlet of the upstream APS and the wind tunnel results in anisokinetic sampling for the upstream APS. This impact was accounted for the same way as described previously using the diameter of inlet tube of 1.93cm. It causes the significant change for net enhancement correction for the data (Figure 14, Figure 15, Figure 16). When wind speed is 1m/s, the value of anisokinetic factor is below 1. For wind speed is 3m/s or 4.5m/s, the value is higher than 1.

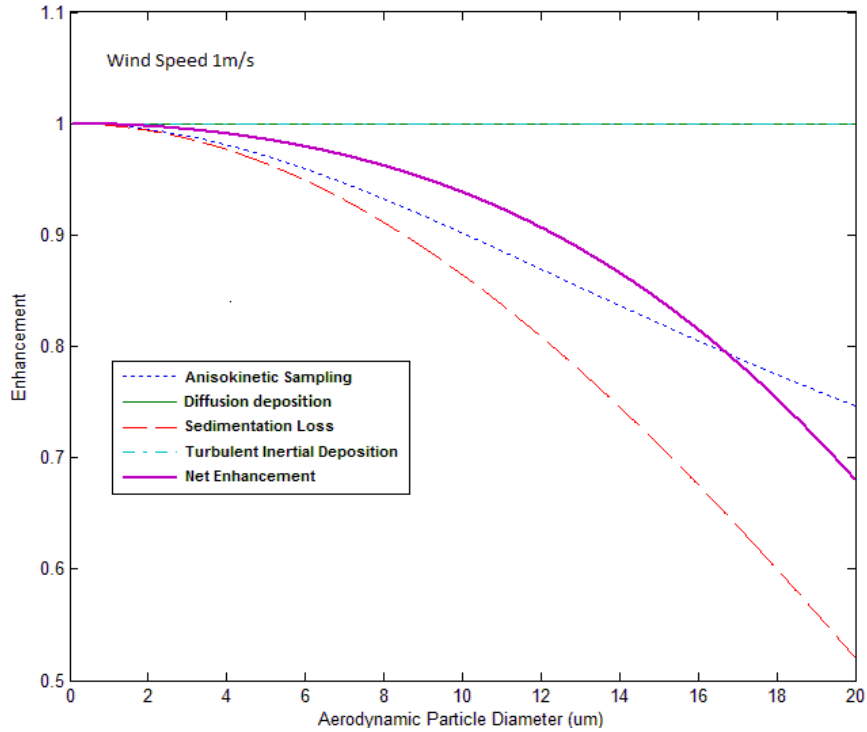


Figure 14. Enhancement factors for the upstream APS at a wind speed of 1 m/s.

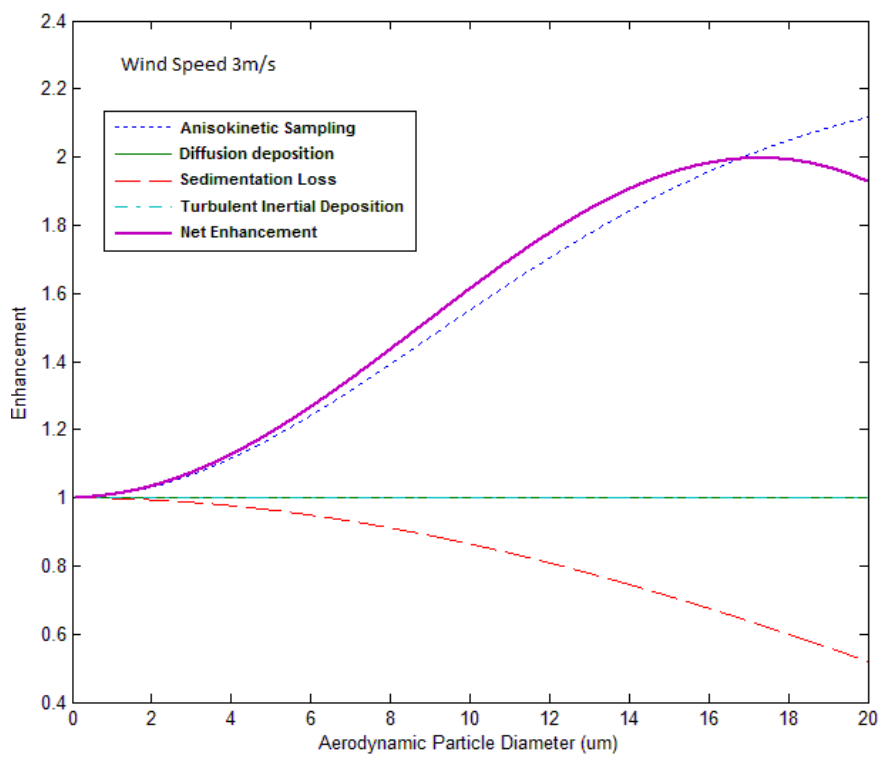


Figure 15. Enhancement factors for the upstream APS at a wind speed of 3 m/s. Diffusional and turbulent inertial deposition corrections are not significant for the conditions encountered in these experiments.

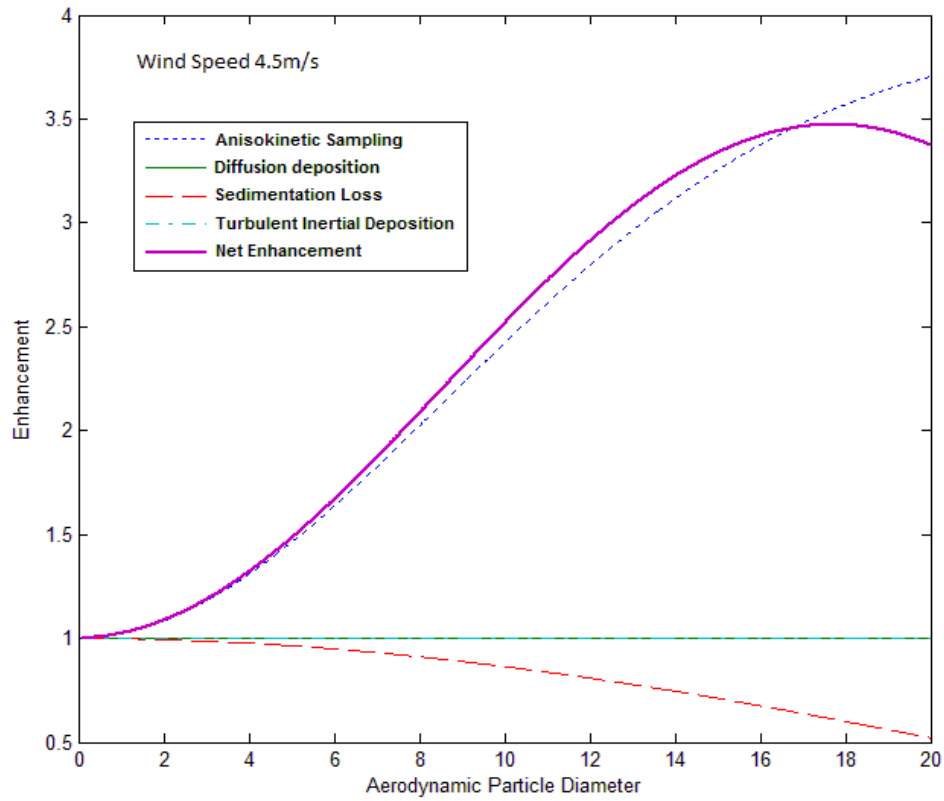


Figure 16. Enhancement factors for the upstream APS at a wind speed of 4.5 m/s. Diffusional and turbulent inertial deposition corrections are not significant for the conditions encountered in these experiments.

**<u>Conversion of APS number concentrations to mass concentrations</u>**

The data from the APS are based on aerodynamic diameter, assuming unit density (1gm/cm$^3$) of particles. The mass concentrations are obtained from APS data by:

$$M_{APS} = \pi \frac{\rho_0 D_{ae}^3}{6} \qquad \text{Eqn 18}$$

where $M_{APS}$ is single particle mass, $\rho_0$ is particle density (if aerodynamic diameter is used, $\rho_0$ = 1g cm$^{-3}$) and $D_{ae}$ is particle aerodynamic diameter.

For non-spherical particles experiencing the same drag force as spherical particles, we have:

$$\rho_p D_e^2 = \rho_0 D_{ae}^2 \chi \qquad \text{Eqn 19}$$

where $\rho_p$ is the particle bulk density, $D_e$ is the volume equivalent diameter and $\chi$ is shape factor of non-spherical particles. By combining equations [18] and [19], the real particle mass can be converted from the APS data:

$$M_p = \pi \frac{\rho_0 D_e^3}{6} = M_{APS}\sqrt{\frac{\rho_0 \chi}{\rho_p}} \qquad \text{Eqn 20}$$

For compact non-spherical particles, the shape factor is usually less than 1.5. If the fugitive particles are mostly silica, the density would be about 2.5g/cc.

The theoretical anisokinetic enhancement values can be compared to experimental obtained enhancement factors, considering the exact geometry of our setup – which is referred to here as the elbow correction factor. For these experiments, particle concentration measurements were made with the upstream and downstream APS instruments in a chamber without any flow. The downstream APS sub-sampled from a high flow elbow region, as before, but without the LPI in place. A comparison of experimental and theoretical elbow factors for a LPI sampling volume of 820 LPM, suggests that the downstream APS samples largely as expected theoretically, with a small deviation between 4 and 10 µm (Figure 17).

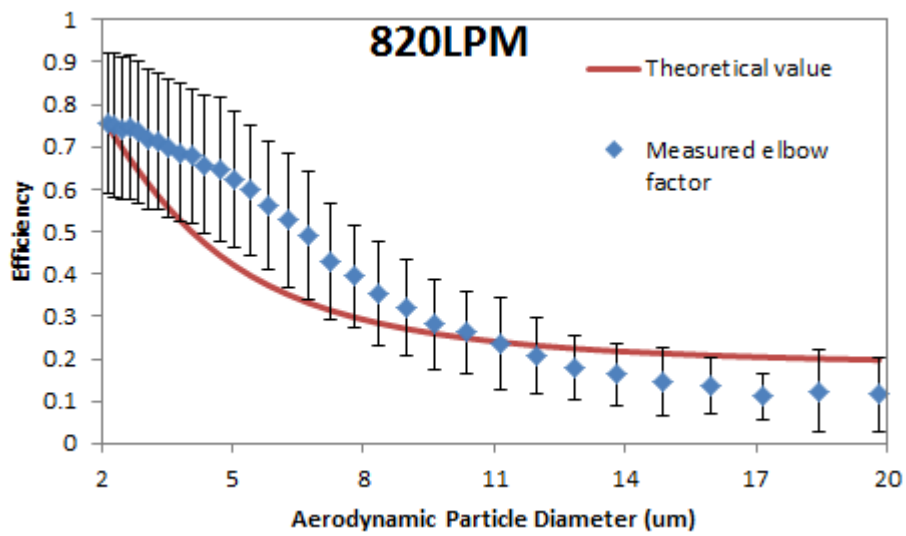


Figure 17. Experimental and theoretical elbow factors. Efficiency was calculated by dividing the upstream data by the downstream data (flow rate=820LPM). Error bars indicate one standard deviation.

**Upstream APS: Net Enhancement factor**. The upstream APS samples from the wind-tunnel with velocity different from the freestream and with a sampling tube of length ~ 25 cm in front of the inlet. To obtain the freestream particle size distribution from the upstream APS measurements, the particle transport losses in the finite length of the sampling tube must be calculated and the anisokinetic sampling effect, resulting from a mis-match between the freestream and sampling velocity, must also be accounted for. The different loss mechanisms vary with particle size and wind speed. The net enhancement calculated as a product of all the loss factors and the anisokinetic enhancement is also shown in Figure 18 and for large particles is <1 at 1 m/s wind speed and >1 at 3 m/s wind speed.

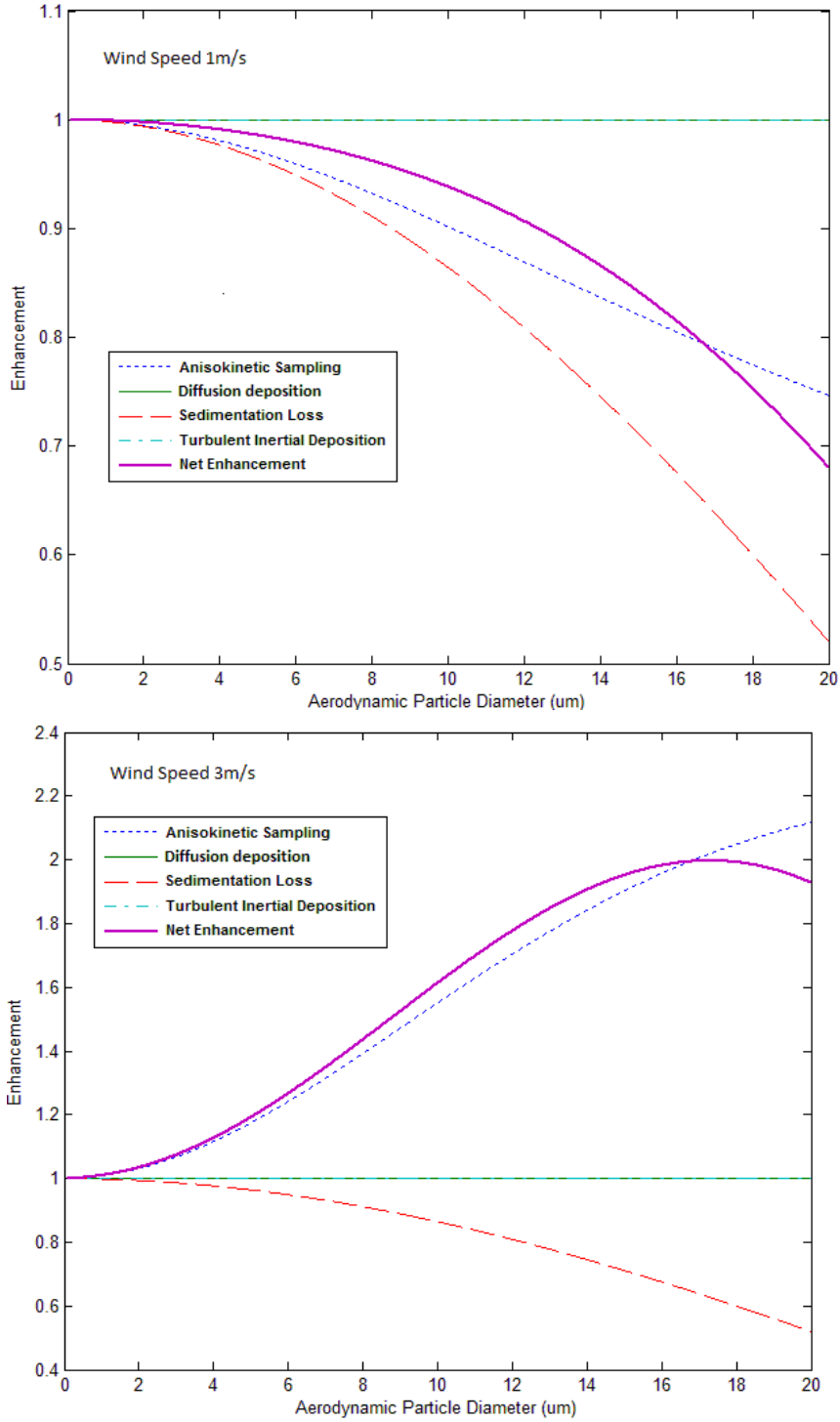


Figure 18. Enhancement factors for the upstream APS at a wind speeds of 1 and 3 m/s.

**Comparison of Experimental and Numerical Results.**

With the above-described corrections to the upstream and downstream APS measurements, the experimental LPI sampling efficiency can be calculated as a ratio of these measurements. For

comparison with the numerical modeling results of LPI sampling efficiency presented in Lee et al., (2008), however, one additional consideration must be made. The numerical results of Lee et al., (2008) were obtained considering the total number of particles collected over the entire exit of the LPI. In the current wind-tunnel experiments, only particles close to the central region of the LPI exit were measured by the downstream APS (as illustrated by the location of the downstream APS sample tube in Figure 13). The numerical results of Lee et al., (2008) were re-analyzed as part of this study and the spatial distribution of particles at the exit of the LPI were obtained as a function of their size. Particles of different sizes travel through different paths in the LPI and CFD simulation results of the spatial distribution of particles of 4 different sizes at the LPI exit are shown in Figure 19. It is observed that larger particles are more concentrated in the center along the wind direction (left to right).

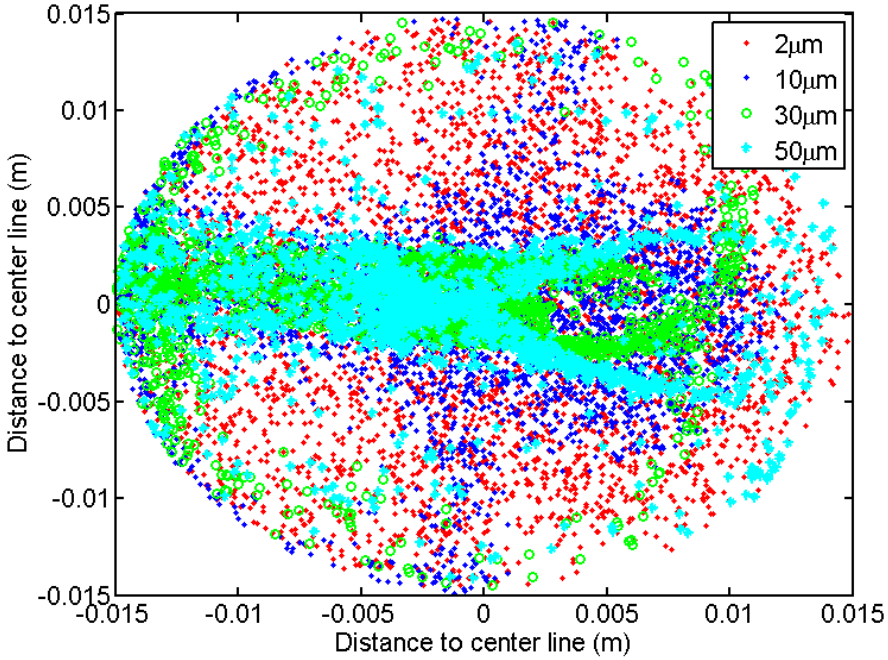


Figure 19. Particle locations in a cross section of tubing downstream of the inlet at 820 LPM showing particles of larger size are not uniform within the sampling tube cross-section.

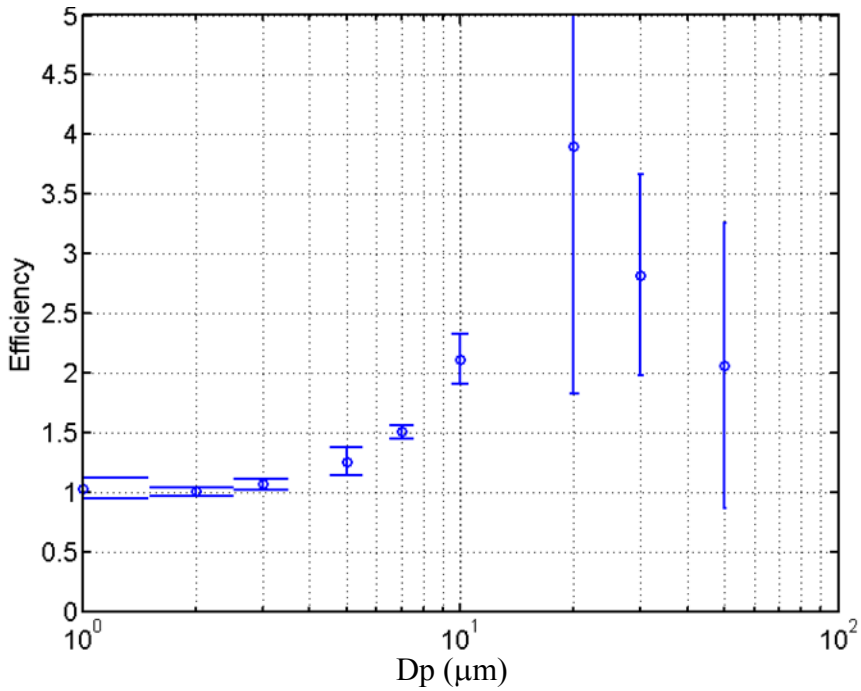


Figure 20. The particle concentration enhancement at central locations downstream of the inlet at 820 LPM. Dp is particle diameter.

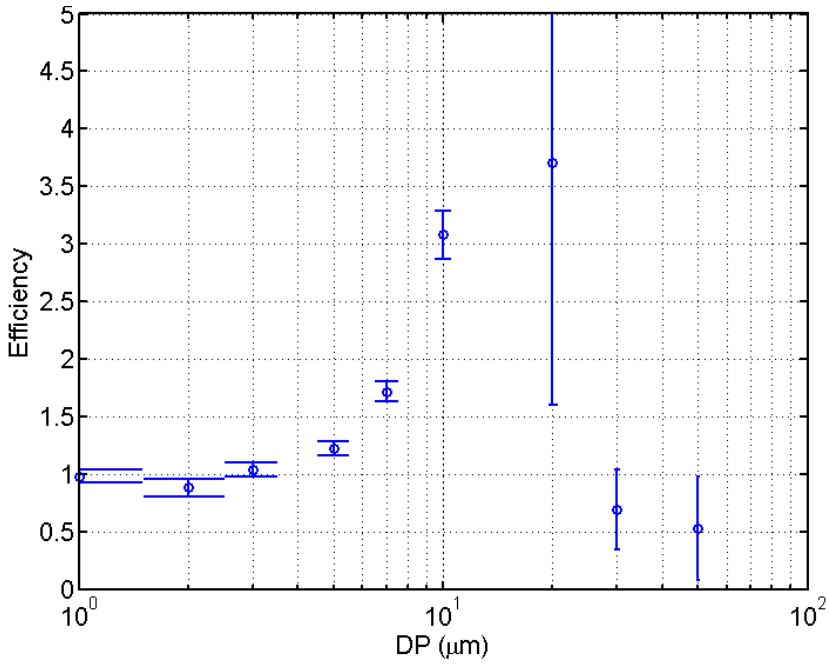


Figure 21. The particle concentration enhancement at central locations downstream of the inlet at 1750 LPM.

The particle concentrations at the center of the exit were obtained as an average of concentrations at five sampling locations around the center of the exit section. The diameters of the 5 locations were chosen as 5 mm corresponding to a region approximately proportional to the sampling flowrate of the APS. The calculated sampling enhancements in the central region of the LPI exit for sampling flow rates of 820 and 1750 LPM are shown in Figures 20 and 21.

**Overall results of LPI sampling efficiency tests.** A comparison of the numerical results with the experimental measurement of LPI efficiency using the two APS instruments and wind-tunnel based testing is shown in Figures 22 and 23.

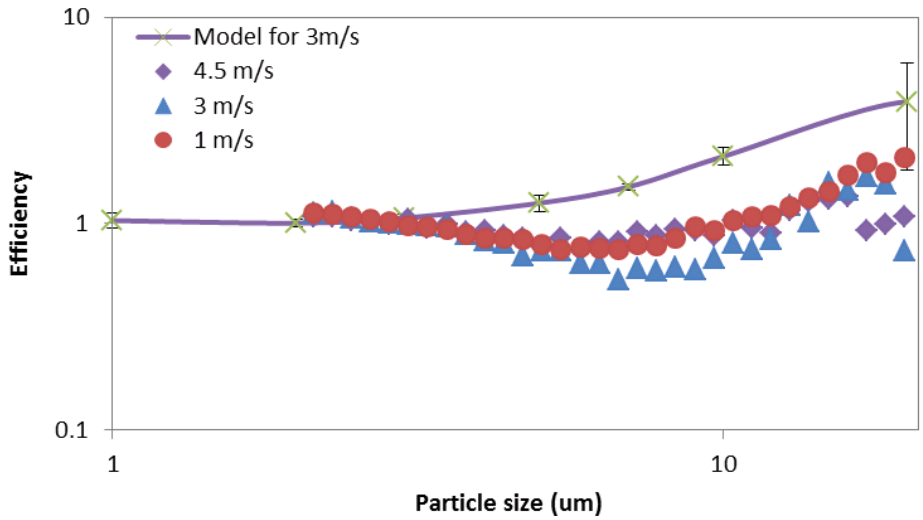


Figure 22. A comparion of the numerically predicted inlet enhancements with the experimentally measured values for a sampling flow rate of 820 LPM. The experimental data are corrected for all the measurement non-idealities described above. Error bars indicate one standard deviaiton

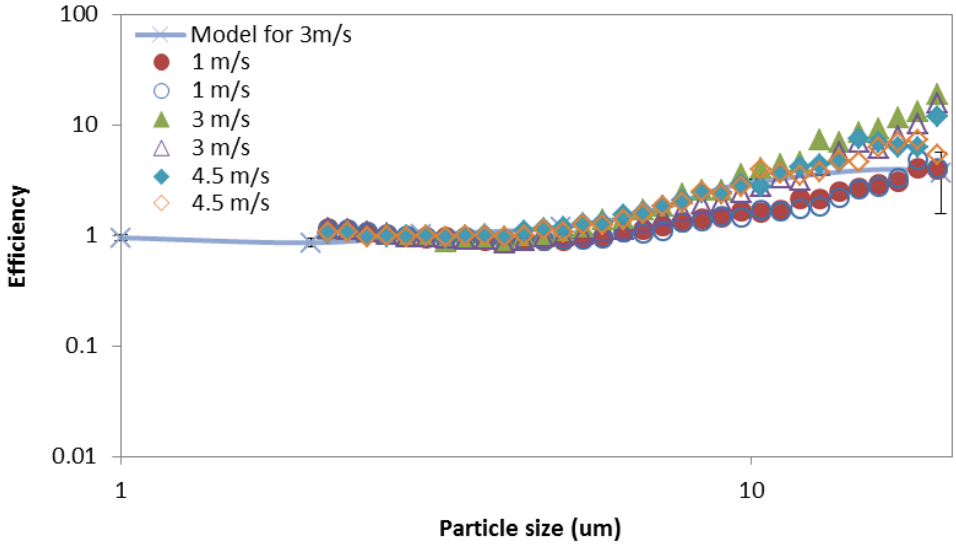


Figure 23. A comparison of the numerically predicted inlet enhancements with the experimentally measured values for a sampling flow rate of 1750LPM. The experimental data is

corrected for all the measurement non-idealities described above. Error bars indicate one standard deviation.

For a high LPI sampling flowrate (1750 LPM). the numerical and experimental results are largely matched. At a lower sampling flowrate of 820 LPM, the general trends of the theoretical and numerical sampling efficiency curves are similar, but there is about a factor of two discrepancy. This discrepancy can likely be accounted for, if additional non-idealities are considered, such as: 1) the effect of the finite size of the downstream APS sampling tube within the elbow, 2) additional mixing between the exit of the LPI and the 12 inch of flow length prior to sampling by the downstream APS sub-sample tube in the elbow and 3) the loss of particles at the entrance to the sub-sample tube.

Additional experiments will be required to consider these secondary effects.

**Field Validation of LPI-FM-100.**

Three real-time instruments were used in this experiment. The LPI-FM-100 measured the optical size distribution, the APS measured aerodynamic size distribution and the Dusttrak measured the $PM_{2.5}$ mass concentration based on a precalibration with a standard. An example of a typical particle concentration time series from the APS and LPI-FM-100 instruments are shown in Figure 24. The particle concentrations are colored in a log-scale to capture the broad range of concentration values measured during the observation period.

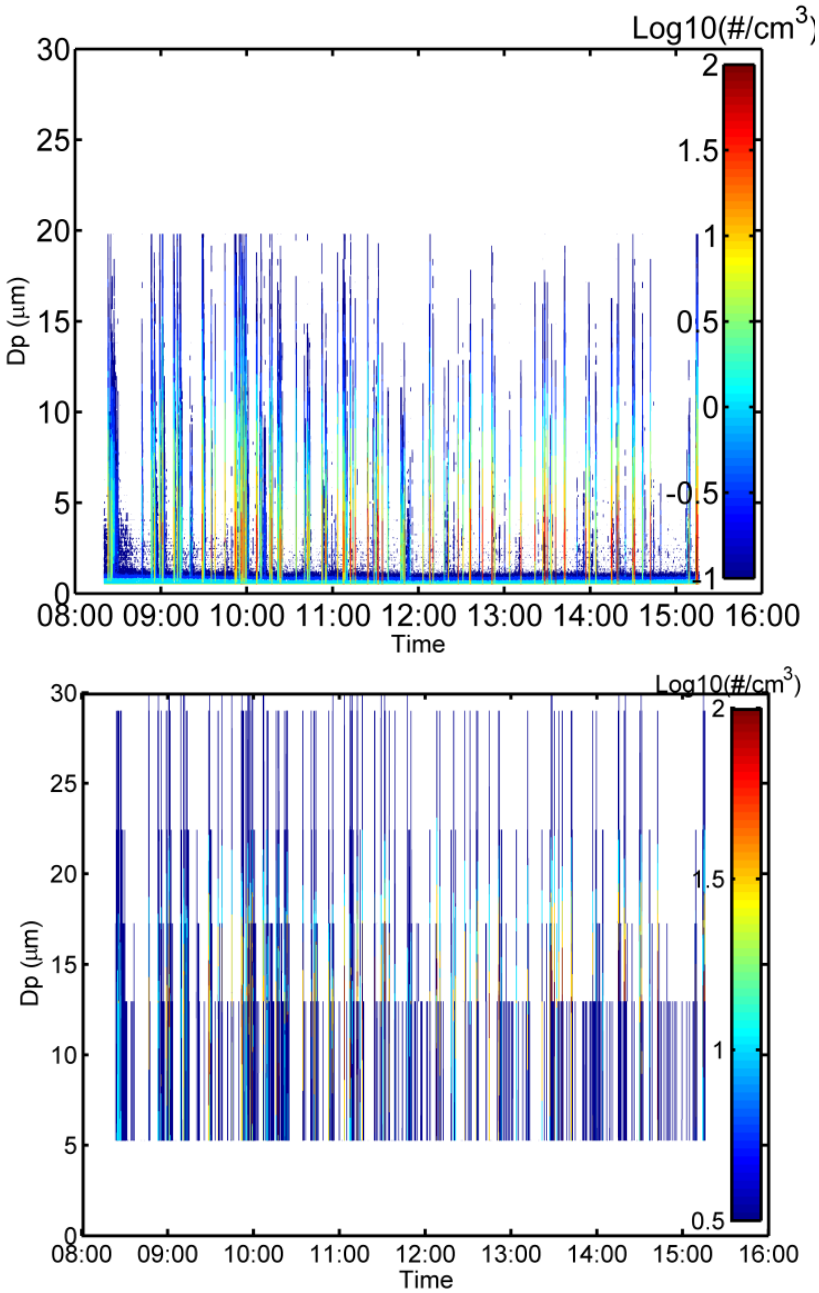


Figure 24. Time series of measured size distribution from APS and FM-100. (Aug. 27th). (a) Contour plot of APS data; (b) Contour plot of FM-100 data. Note that the data for both the instruments are plotted in equivalent aerodynamic diameter. A refractive index of 1.51 is used in calculating optical sizes with the FM-100.

During the measurement time, there were periods of low particle concentrations corresponding to traffic-free conditions interspersed with high concentration periods that were linked to local traffic. During these periods the concentrations quickly returned to background levels after the traffic passed. To enable a direct comparison of the size distribution measurements made with the LPI-FM-100 with those made by an APS instrument, the optical sizes from the LPI-FM-100 are converted to aerodynamic sizes by considering particles with refractive index of 1.51 and

particle density of 2.5 gm $cm^{-3}$ (consistent with properties of dust particles). The LPI-FM-100 size distributions suggest the presence of particles as large as 30 μm in locations near unpaved roads during times of traffic movement. The number size distribution obtained from the real-time instruments can be converted to a mass concentration time series as shown in Figure 25 for one measurement day.

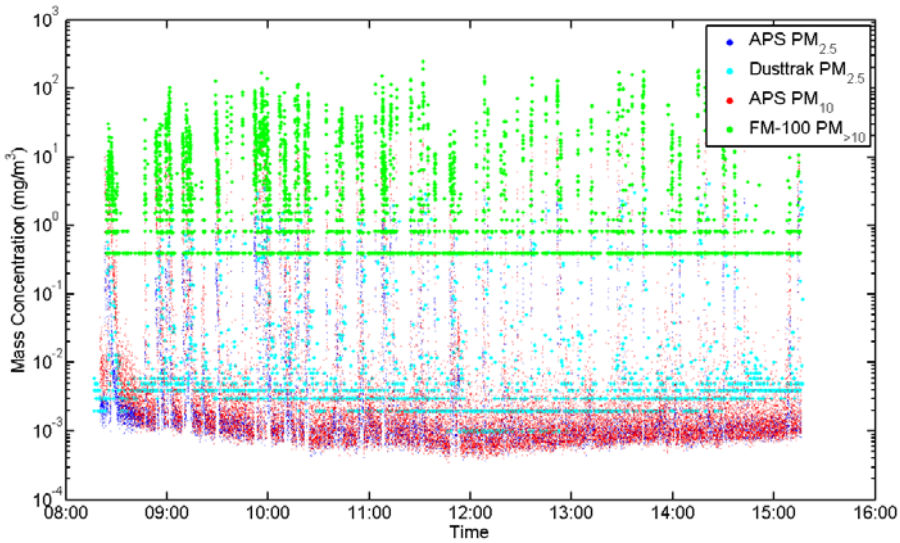


Figure 25. Particle mass concentration during a day (Aug. 27th).

The ability of the FM-100 instrument to detect large particles was established with lab experiments, as discussed in the "Materials and Methods" section. To validate the performance of the integrated LPI-FM-100 instrument in detecting the concentration of particles larger than 10 μm, field measurement results are used. The daily averaged mass concentrations determined from the LPI-FM-100 measurements are compared to that obtained with traditional filter-based measurements. The $PM_{>10}$ filter-based values are obtained as a difference between the total suspendend particulate (TSP) and $PM_{10}$ concentrations (referred to as TSP – $PM_{10}$). A comparison of the filter-based measurements of $PM_{>10}$ with that obtained from the real-time LPI-FM-100 instrument is shown in Figure 26. It is observed that there is a good match between the measurements made by the two techniques providing initial validation of the performance of the integrated LPI-FM-100 instrument for measurement of particles larger than 10 μm. Some discrepancy between the two measurements could possibly be because of the day-to-day variation in ambient wind-speeds. In Figure 27, the ratio of the $PM_{>10}$ measurements from the two techniques are compared against the average wind-speeds during the different days of measurement. It is observed that the $PM_{>10}$ measurements with the LPI-FM-100 increase relative to the filter based values as the average wind-speeds increase. This observation suggests that the $PM_{>10}$ measurements with the filter-based instruments are likely to be biased-low under high wind-speed.

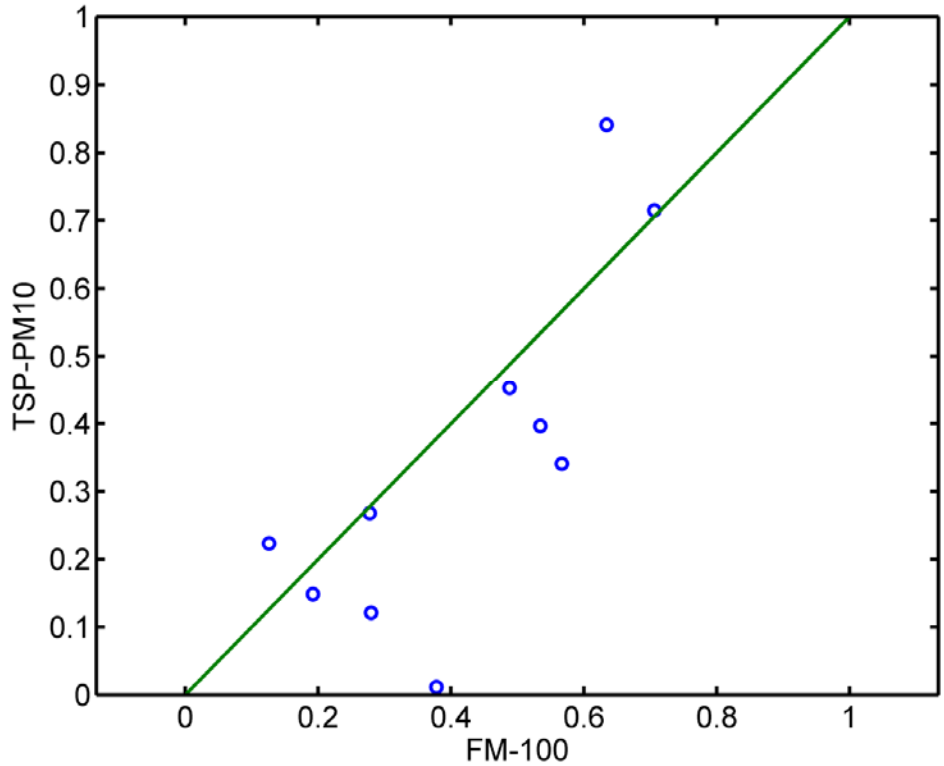


Figure 26. A comparison of $PM_{>10}$ measurements make by the LPI-FM-100 instrument and the filter based technique ($TSP\text{-}PM_{10}$).

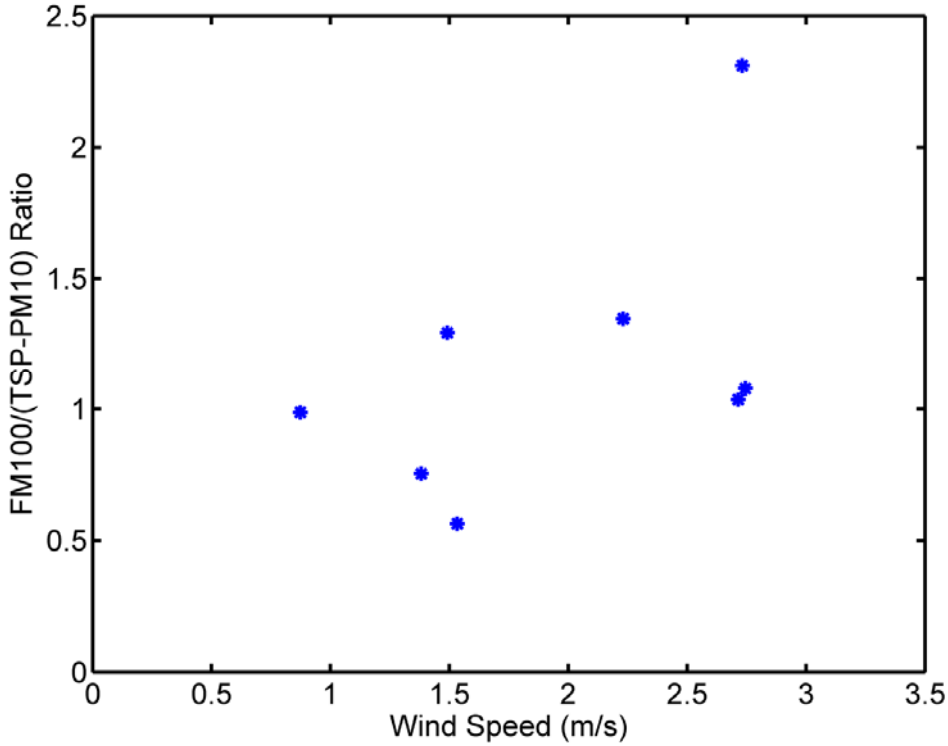


Figure 27. The ratio of PM>10 measurements made by the LPI-FM-100 and the filter-based technique (TSP-PM10) as a function of wind speed.

**Field measurements of fugitive dust size distributions.**

Several instruments were utilized in the field campaign. The filter-based devices yield one data point per day (mass/volume) and the real-time instruments measure on a short timescale and generally yield particle number/volume data by size. The real-time information from the APS and LPI-FM-100 instruments were analyzed to determine the typical background and fugitive dust characteristics. The total and background 10-day average particle number size distributions, obtained from the APS and LPI-FM-100 instruments, are shown in Figure 28. As expected the majority of the measured particles were < 10 μm in size although there were particles measured in the largest size bin of the LPI-FM-100. The background concentrations in the measured sites was ~ 15 particles $cm^{-3}$ for most of the days and ~ 150-200 particles $cm^{-3}$ for the last two days.

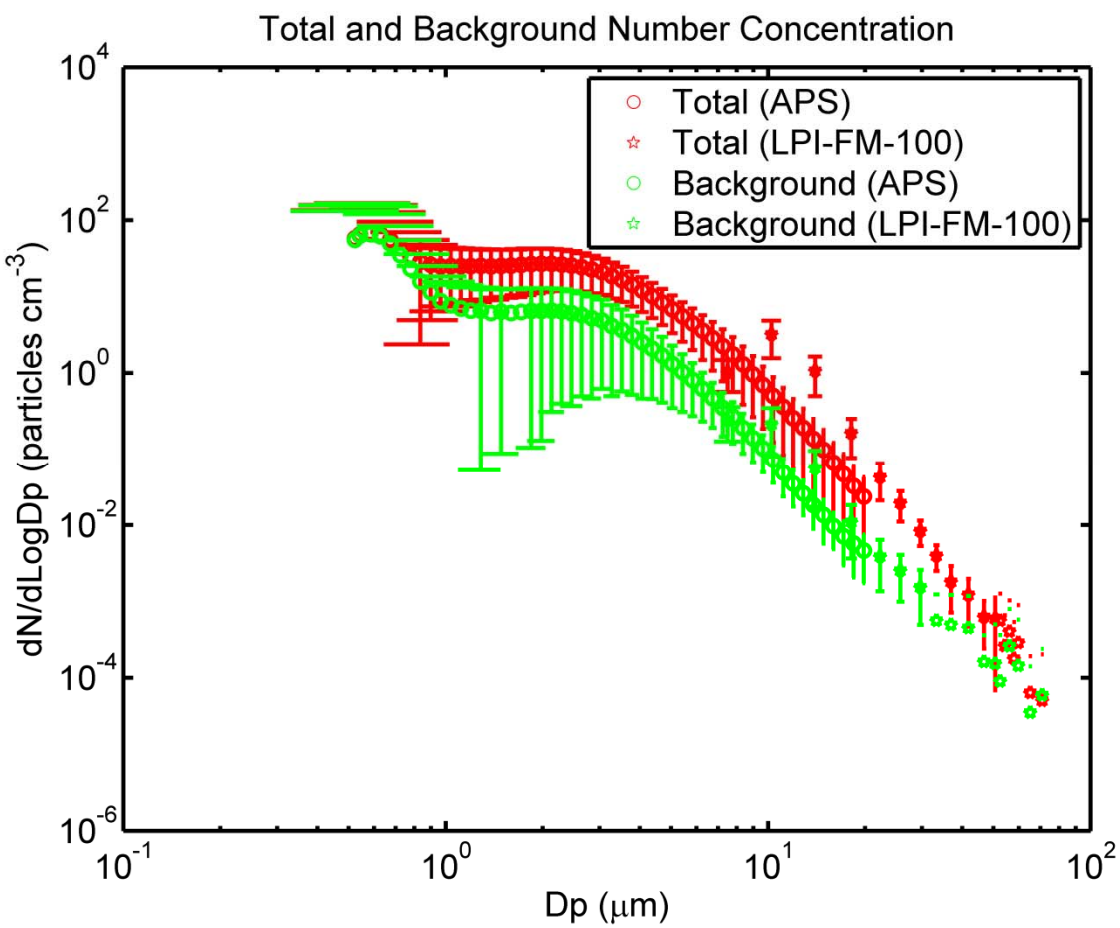


Figure 28. The average total and background particle number size distribution. Particle diameters are aerodynamic diameters for APS and optical diameters for LPI-FM-100.

The total and background mass concentrations are shown in Figure 29. The mass size distribution is bi-modal in shape with approximately 40%-50% of the mass less than 2 μm in size. Assuming a particle bulk density of 1.3 gm $cm^{-3}$ the mass distribution measured by the APS and LPI-FM-100 data agree fairly well. This value of particle bulk density deviates from that expected for dust particles (~ 2.0-2.5 gm $cm^{-3}$) however we have adjusted just the particle

density value to match the data, ignoring the complex integrated influence of particle shape and density in both optical and aerodynamic size measurements.

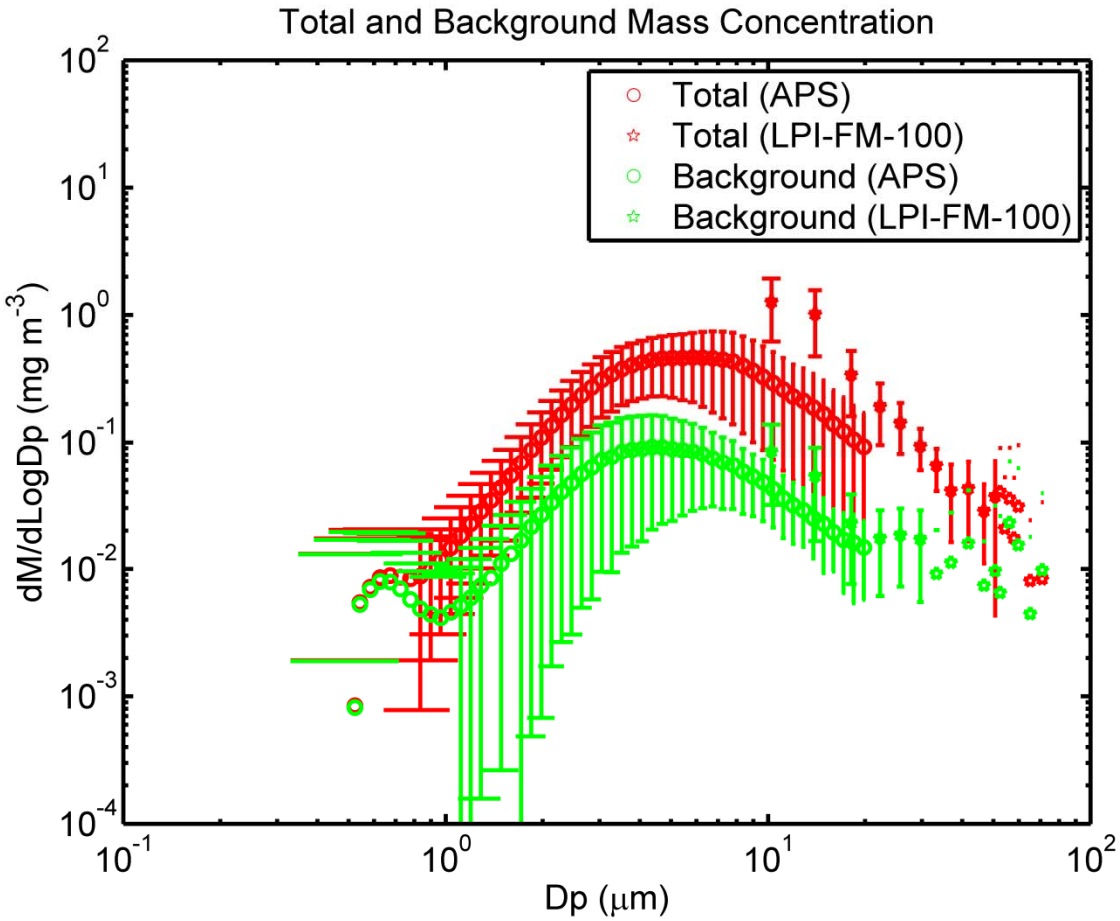


Figure 29. Total and background mass concentration averaged during 10 days. Mass was calculated based on aerodyanmic diameter and unit density for APS, optical diameter and 2 gm/cm$^3$ for LPI-FM-100.

A first estimation of the fugitive number and mass distribution was obtained from the difference of the background and high concentration periods (Figures 30 and 31). This fugitive dust size distribution is mono-modal with a peak at approximatley 8 μm. The fugitive dust size distributions suggest ~20% of the mass is associated with particles in sizes larger than 10 μm and ~ 5% is associated with particles in sizes larger than 20 μm.

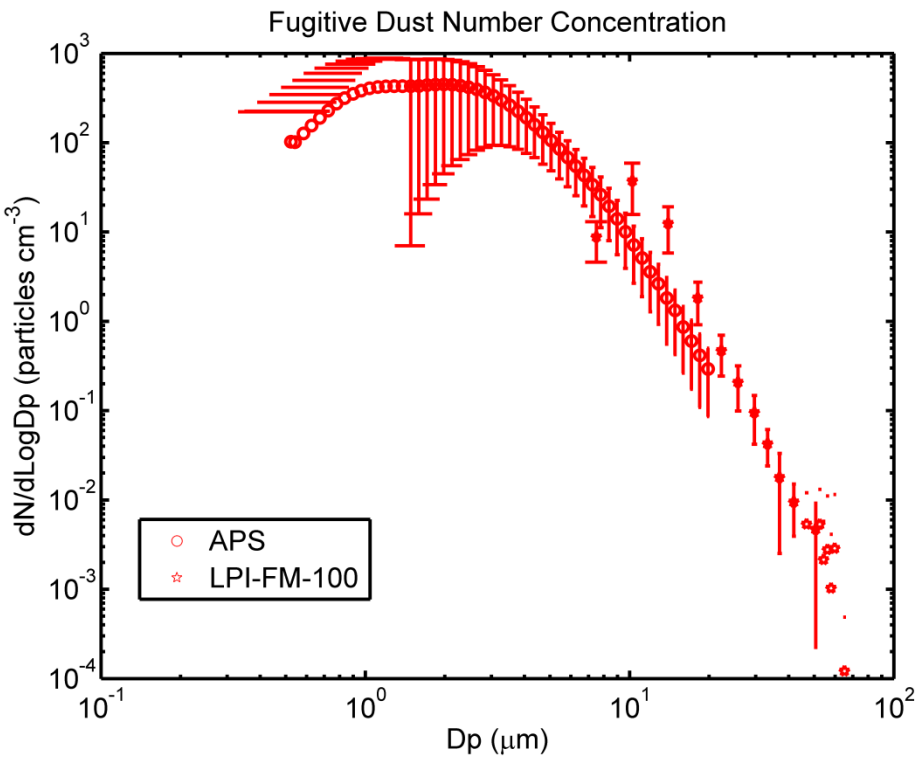


Figure 30. The fugitive dust number distribution, averaged for 10 days.

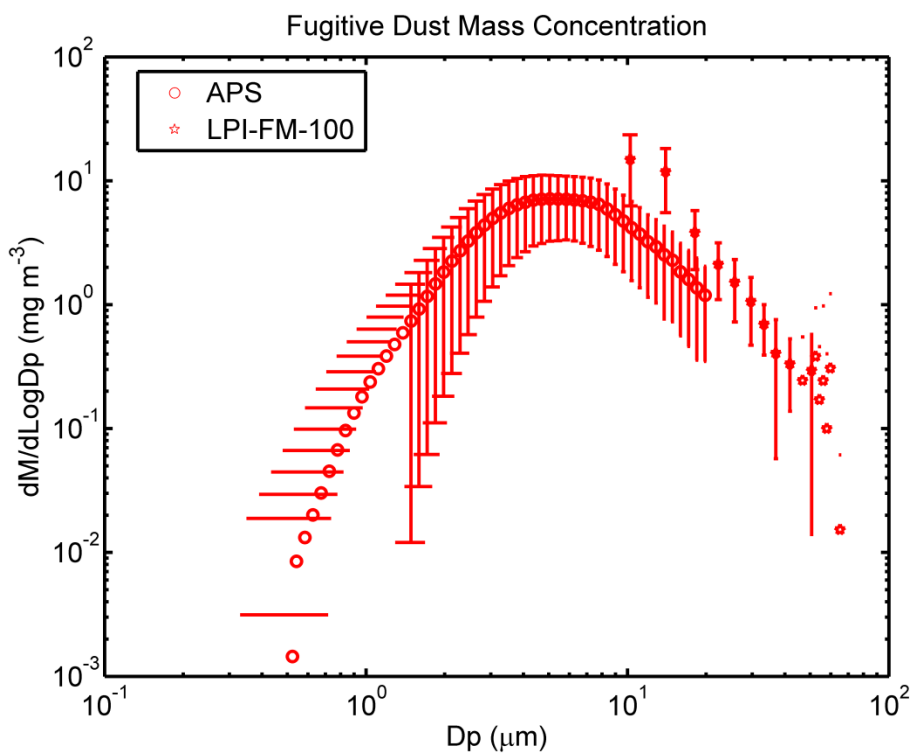


Figure 31. The fugitive dust mass distribution, averaged for 10 days.

## Conclusions and Implications for Future Research

The outcome of this project was the development of a real-time instrument (LPI-FM-100) capable of real-time measurement of fugitive dust particles over a size range of 2 to 73 μm (mean bin sizes: 4, 7.5, 10.5, 13.5, 16.5, 19.5, 22.5, 25.5, 28.5, 33, 36, 40, 44, 48, 52, 56, 60, 64, 68, and 73 μm). This instrument consists of a commercially available fog monitor (FM-100; Droplet Measurement Technologies, Boulder CO) connected to an carefully designed and characterized inlet (LPI) that can sample large particles typically lost in traditional samplers. As the LPI samples omni-directionally, its sampling characteristics are largely independent of wind direction. The sampled particles are exited vertically and measured with the FM-100 instrument. This new integrated setup (LPI-FM-100) was characterized in a wind-tunnel and in the field.

Laboratory experiments with glass beads showed that the FM-100 was able to measure particles into the 20 size bins listed above. The average sizes measured by the FM-100 were consistent with those obtained from a Mastersizer 2000 (Malvern Instruments). The size distributions obtained from the two instruments, however, differed in the lower and higher limits of the distribution. Relative to the Mastersizer measurements, the FM-100 size distributions show a greater number of particles smaller than the mean size and fewer number of particles larger than the mean size. This discrepancy is likely because of the different dispersion mechanisms used for the two samples. For the Mastersizer measurements, particles were placed into water and dispersed using a ultrasonic bath, while the particles were dispersed into the FM-100 using a compressed air source, which is likely to result in a higher dispersion efficiency of smaller particles than larger particles.

Wind tunnel measurements found that the sampling efficiencies of the LPI were largely consistent with predictions. For a high LPI sampling flowrate (1750 LPM), the numerical and experimental results are in reasonable agreement. At a lower sampling flowrate of 820 LPM, the general trends of the theoretical and numerical sampling efficiency curves are similar, but there is about a factor of two difference. This discrepancy can likely be accounted for considering additional non-idealities. As the wind-tunnel experiments required two identical sizing instruments for upstream and downstream measurements and only APS units were available for such measurements, the LPI wind-tunnel tests were limited to particle aerodynamic sizes smaller than 20 μm.

During field evaluations the measurements revealed that there were periods of low particle concentrations corresponding to traffic-free conditions interspersed with high concentration periods that were linked to local traffic. After these periods the concentrations quickly returned to background levels. In the overlap size range, the LPI-FM-100 size distributions were largely consistent with those measured using another real-time instrument (APS). The LPI-FM-100 consistently detected the presence of particles in all size bins during times of traffic movement, but the concentration of particles >30 μm was generally very low. These measurements enabled a first estimation of the fugitive number and mass distribution by using the difference of the background and high concentration periods. This fugitive dust size distribution is mono-modal with a peak at approximatley 8 μm. The fugitive dust size distributions suggest ~20% of the mass is associated with particles in sizes larger than 10 μm and ~ 5% is associated with particles in sizes larger than 20 μm. A comparison of the filter-based and LPI-FM-100 $PM_{>10}$ values found there is a reasonable match between the measurements made by the two techniques

Although the results of this project have resulted in a well characterized instrument there are a few sampling non-idealities that were not accounted for, such as: 1) the effect of the finite size of the downstream APS sampling tube within the elbow, 2) additional mixing between the exit of the LPI and the 12 inch of flow length prior to sampling by the downstream APS sub-sample tube in the elbow and 3) the loss of particles at the entrance to the sub-sample tube. Additional CFD work in combination wind tunnel measurements would result in a better characterized sampler.

One of the limits of the LPI-FM-100 instrument is that it does not measure the smaller particles that make up most of the particle number of the fugitive dust signal. This shortcoming will limit the usefulness of LPI-FM-100 as a stand-alone fugitive dust monitor. An instrument that combines the LPI-FM-100 with an APS would allow the measurement of the complete size distribution of the fugitive dust signal in real-time as is needed for model development and validation. Such an instrument, if carefully designed, could limit many of the non-idealities that had to be accounted for in this project. In designing such an instrument, care must be taken to ensure that the differences in particle number concentration detection limits of the two instruments are accounted for. The new instrument could control the flow downstream of the LPI-FM-100 so that the APS sampling is isokinetic and the concentrations are low enough that the APS is not overloaded. In addition, the APS will have to be in a weather-proof enclosure so this instrument could be used in the field. Deployment of such an instrument for fugitive dust measurement will enable accurate, real-time size and mass distribution measurements over the entire particle diameter range of interest and provide critical data towards validation of advanced fugitive dust models being developed.

## References


Baron, P. A. and Willeke, K., 2001. Aerosol Measurement - Principles, Techniques, and Applications (2nd Edition), John Wiley & Sons

Belyaev, S.P., and Levin, L. M., 1974. Techniques for collection of representative aerosol samples, *Journal of Aerosol Science*, 5, 325-338.

Chow, J. C., Watson, J. G., Houck, J. E., Pritchett, L. C., Rogers, C. F., Frazier, C. A., Egami, R. T. and Ball, B. M., 1994. A laboratory resuspension chamber to measure fugitive dust size distributions and chemical compositions. *Atmos. Environ.* 28:21, 3463-3481.

Dhaniyala, S., Flagan, C. R., McKinney K. A., and Wennberg, P.O., 2003. Novel aerosol/gas inlet for aircraft-based measurements, *Aerosol Sci. Technol.*, 37, 828-840.

EPA, Compilation of Air Pollutant Emission Factors, Volume 1: Stationary Point and Area Sources, AP-42, Fifth Edition, U.S. Environmental Protection Agency, Office of Air Quality Planning and Standards, Research Triangle Park, North Carolina, January, 1995.

EPA AP 42, Fifth Edition Compilation of Air Pollutant Emission Factors, 1995. Volume 1: Stationary Point and Area Sources. http://www.epa.gov/ttn/chief/faq/ap42faq.html

Falerios, M., Schild, K., Sheehan, P., Paustenbach, D., 1992. Airborne concentrations of trivalent and hexavalent chromium from contaminated soils at unpaved partially paved commercial/industrial sites. *J. Air Waste Manage. Assoc*. 42: 40-48.

Gysels, K., and Grieken R. V., 1999. Field evaluation of a wind tunnel-impactor system for sampling ambient aerosols, *Journal of Aerosol Science*, 30 (5), 639-650.

Hangal S. and Willeke K., 1990. Aspiration efficiency: Unified model for all forward sampling angles. *Environ. Sci. Technol.* 24, 688-691.

Houck, J. E., Chow, J. C., Watson, J. G., Simons, C. A., Pritchett, L. C., Goulet, J. M.and Frazier, C. A., 1989. Determination of particle size distribution and chemical composition of particulate matter from selected sources in California: volume I and executive summary (final report). Sacramento, CA: California Air Resources Board.

Houck, J. E., Goulet, J. M., Chow, J. C., Watson, J. G. and Pritchett, L. C., 1990. Chemical characterization of emission sources contributing to light extinction. In: Mathai, C. V., ed. Visibility and fine particles: an A&WMA/EPA international specialty conference; October 1989; Estes Park, CO. Pittsburgh, PA: Air & Waste Management Association; pp. 437-446. (A&WMA transactions series no. TR-17).

Gormley, P. G., and Kennedy, M., 1949. Diffusion from a stream flowing through a cylindrical tube. *Proceedings of the Irish Academy*, 52A, 163.

Kitsa, V.and Lioy, P. J., 1992. Near field dispersion of mechanically resuspended dust from an unpaved road. *Transactions AWMA*. 1: 199-210.

Kitsa, V., Lioy, P. J., Chow, J. C.,Watson, J. G.,Shupack, S., Howell, T. and Sanders, P., 1992. Particle-size distribution of chromium: total and hexavalent chromium in inspirable, thoracic, and respirable soil particles from contaminated sites in New Jersey. *Aerosol Sci. Technol.,* 17: 213-229.

Lee, S.R., Dhaniyala S, and Holsen, T.M., 2008. Design and Development of Novel Large Particle Inlet for PM larger than 10 μm (PM>10), *Aerosol Sci and Tech.*, 41(1).

Liu, B.Y.H., Agarwal, J.K., 1974. Experimental observation of aerosol deposition in turbulent flow. *Journal of Aerosol Science*. 5, 145-155.

Pastuszka, J. S. and Kwapulinski, J., 1988. The change in mass size distribution of aerosol near dumps as a result of resuspension of dust. Presented at: 81st annual meeting of Air Pollution Control Association; June; Dallas, TX. Pittsburgh, PA: Air Pollution Control Association; paper no. 88-151.3.

Pich, J., 1972. Theory of gravitational deposition of particles from laminar flows in channels. *Journal of Aerosol Science,* 3, 351–361.

Vincent, J. H., 1989. *Aerosol sampling: Science and practice*, Chichester, UK, Wiley

Williams, D.S., Scott, D., Shuklaa, M.K., Ross, J., 2008. Particulate matter emission by a vehicle running on unpaved road. *Atmospheric Environment*, 42, 3899–3905

# APPENDIX A: Publications

No publications or presentations have been made as part of this work; however a poster summarizing this work will be presented at the American Association for Aerosol Research (AAAR) Conference in Orlando Florida in October 2011. In addition several journal papers are planned.